Basin Research

IAS EAGE

Basin Research (2012) **24**, 520–543, doi: 10.1111/j.1365-2117.2012.00543.x

Late Cretaceous-Palaeogene stratigraphic and basin evolution in the Zhepure Mountain of southern Tibet: implications for the timing of India-Asia initial collision

Xiumian Hu,* Hugh D. Sinclair,† Jiangang Wang,* Hehe Jiang* and Fuyuan Wu‡

**State Key Laboratory of Mineral Deposits Research, School of Earth Sciences and Engineering, Nanjing University, Nanjing, China*

†*School of GeoSciences, The University of Edinburgh, Edinburgh, UK*

‡*Institute of Geology and Geophysics, Chinese Academy of Sciences, Beijing, China*

ABSTRACT

This article presents combined stratigraphic, sedimentological, subsidence and provenance data for the Cretaceous–Palaeogene succession from the Zhepure Mountain of southern Tibet. This region records the northernmost sedimentation of the Tethyan passive margin of India, and this time interval represents the transition into continental collision with Asia. The uppermost Cretaceous Zhepure Shanpo and Jidula formations record the transition from pelagic into upper slope to delta-plain environments. The Palaeocene–lower Eocene Zongpu Formation records a carbonate ramp that is overlain by the deep-water Enba Formation (lower Eocene). The upper part of the Enba Formation records shallowing into a storm-influenced, outer shelf environment. Detrital zircon U–Pb and Hf isotopic data indicate that the terrigenous strata of the Enba Formation were sourced from the Lhasa terrane. Unconformably overlying the Enba Formation is the Zhaguo Formation comprising fluvial deposits with evidence of recycling from the underlying successions. Backstripped subsidence analysis indicates shallowing during latest Cretaceous-earliest Palaeocene time (Zhepure Shanpo and Jidula formations) driven by basement uplift, followed by stability (Zongpu Formation) until early Eocene time (Enba Formation) when accelerated subsidence occurred. The provenance, subsidence and stratigraphy suggest that the Enba and Zhaguo formations record foredeep and wedge-top sedimentation respectively within the early Himalayan foreland basin. The underlying Zongpu Formation is interpreted to record the accumulation of a carbonate ramp at the margin of a submarine forebulge. The precursor tectonic uplift during latest Cretaceous time could either record surface uplift over a mantle plume related to the Réunion hotspot, or an early signal of lithospheric flexure related to oceanic subduction, continental collision or ophiolite obduction. The results indicate that the collision of India with Asia occurred before late Danian (*ca.* 62 Ma) time.

INTRODUCTION

The timing of the initial collision between India and Asia remains a matter of considerable debate, with views ranging from *ca.* 70 to *ca.* 35 Ma (Yin & Harrison, 2000; Zhu *et al.*, 2005; Aitchison *et al.*, 2007; Najman *et al.*, 2010). Part of the reason for this debate is that different researchers use different definitions for the initial collision. Some geologists consider the cessation of marine facies as the time of initial collision; consequently, the widely accepted '55 Ma dogma' (Aitchison *et al.*, 2007) for the initial India-Asia collision was deduced from the cessation of marine facies in the Zanskar Himalaya (Garzanti *et al.*, 1987; Garzanti, 2008). Other workers have taken the lower Miocene Gangrinboche conglomerates to constrain the minimum age of the India-Asia collision (Aitchison *et al.*, 2002). These conglomerates are undoubtedly intermontane post-collisional deposits, but are not considered to provide a precise age for the initial stages of the collision (see DeCelles *et al.*, 2011). Here, we follow the definition that the initial India-Asia contact is defined as the time at which the edge of the Indian continent margin first underthrust the Asian trench, leading to the complete consumption of the Neotethyan lithosphere, followed by continental subduction. In this definition, the cessation of marine facies deposition represents the starting of land-to-land (hard) collision time and only provides a minimum age for initial collision.

Correspondence: Dr Xiumian Hu, State Key Laboratory of Mineral Deposits Research, School of Earth Sciences and Engineering, Nanjing University, Nanjing, China.
E-mail: huxm@nju.edu.cn

In southern Tibet, recent palaeomagnetic studies from both sides of the Indus-Yarlung suture zone suggest that the initial contact between India and Asia happened no later than *ca*. 50 Ma (e.g. Tong *et al.*, 2008; Chen *et al.*, 2010; Dupont-Nivet *et al.*, 2010; Huang *et al.*, 2010; Liebke *et al.*, 2010; Najman *et al.*, 2010; Sun *et al.*, 2010; Lippert *et al.*, 2011; Yi *et al.*, 2011); these studies ruled out a model for an Oligocene age of India-Asia collision (e.g. Aitchison *et al.*, 2002, 2007). Cessation of marine facies and the first arrival of Asian detritus occurred around *ca*. 50 Ma both in Tingri and Saga areas of southern Tibet (e.g. Zhu *et al.*, 2005; Najman *et al.*, 2010; Wang *et al.*, 2011), which constrains a minimum age of *ca*. 50 Ma for the India-Asia initial collision. Recently, Cai *et al.* (2011) reported Asia-derived detritus in the 'Upper Cretaceous' Zongzhuo Formation in the northern Tethyan Himalaya in Gyangze. However, the age of the Zongzhuo Formation may not be Late Cretaceous considering that Palaeocene radiolarians were discovered in the matrix of the Zongzhuo succession (Liu & Aitchison, 2002). Furthermore, the Zongzhuo Formation includes mélange or olistoliths clearly showing block-in-matrix structure, which should not be regarded as normal sedimentary strata (see Searle *et al.*, 1987; Liu & Einsele, 1996; Liu & Aitchison, 2002).

In this study, we combine regional stratigraphic and sedimentological data on the Upper Cretaceous to Eocene succession of the Zhepure Mountain in the county of Tingri, southern Tibet, incorporating subsidence analysis and detrital zircon U–Th–Hf isotopic analyses. These data are used to assess the controls on the stratigraphic evolution of the northern margin of India during this important time interval, and the timing of the first arrival of orogenically derived detritus. Implications for the timing of the initial India-Asia collision are considered.

GEOLOGICAL SETTING

The Indus-Yarlung suture zone in southern Tibet, represented by east-west trending exposures of ophiolite and serpentinite-matrix mélange, delineates the contact between the Indian and Asian continents (Fig. 1a) (Hodges, 2000; Dubois-Cote *et al.*, 2005). North of the suture zone is the Lhasa terrane, which can be divided further into the northern, central, and southern subterranes (e.g. Pan *et al.*, 2006; Zhu *et al.*, 2011a). The northern Lhasa subterrane comprises Jurassic–Cretaceous sedimentary and igneous rocks (Pan *et al.*, 2006; Zhu *et al.*, 2009b). The central Lhasa subterrane is dominated by a Carboniferous–Permian metasedimentary sequence and an Upper Jurassic–Lower Cretaceous volcanosedimentary sequence (Kapp *et al.*, 2005; Zhu *et al.*, 2011a). The southern Lhasa subterrane is dominated by the Late Triassic to Palaeogene Gangdese batholith and Palaeogene Linzizong volcanic successions, with minor Triassic–Cretaceous volcanosedimentary rocks (Chung *et al.*, 2005; Chu *et al.*, 2006; Lee *et al.*, 2007, 2009; Mo *et al.*, 2008; Wen *et al.*, 2008; Ji *et al.*, 2009; Zhu *et al.*, 2011a). The Xigaze forearc basin (Fig. 1a), which lies at the southern margin of the Lhasa terrane, is considered to be the forearc to the southern active margin of the Asian plate and comprises Cretaceous (Aptian–Santonian) clastic deep water strata interbedded with scarce marly carbonate layers (Einsele *et al.*, 1994; Dürr, 1996; Wang *et al.*, 1999).

South of the Indus-Yarlung suture zone, the Indian-affinity Himalayan rocks consist of the Tethyan, Greater, and Lesser Himalayas (Fig. 1a). South of the Tethyan Himalaya, separated by the south Tibetan detachment zone (STDZ), are the Greater Himalaya, comprising metamorphosed Proterozoic–Cambrian sedimentary rocks and Cambro-Ordovician orthogneisses. The Main Central Thrust (MCT) separates the Greater Himalaya from the Lesser Himalaya to the south, which consists of Precambrian metasediments metamorphosed from low-grade to amphibolites facies metamorphic conditions (Le Fort, 1989). In the Tansen area of Nepal, the Eocene –lower Miocene foreland basin sedimentary rocks (e.g. DeCelles *et al.*, 1998a; Najman *et al.*, 2005) are located within the Lesser Himalaya (Fig. 1a). South of the Lesser Himalaya is the sub-Himalayan zone (Fig. 1a), consisting of late Cenozoic fluvial foreland basin sedimentary deposits of the Siwalik Group (Critelli & Ingersoll, 1994; DeCelles *et al.*, 1998b).

The Tibetan Tethyan Himalaya is the focus of this analysis, and is generally subdivided into southern and northern zones (Gansser, 1964; Liu & Einsele, 1994; Jadoul *et al.*, 1998) separated by the Gyirong–Kangmar thrust (GKT, Ratschbacher *et al.*, 1994) (Fig. 1b). The southern Tethyan Himalaya is characterized by shallow-water shelf carbonates and terrigenous Palaeozoic to Eocene strata (Liu & Einsele, 1994; Willems *et al.*, 1996; Jadoul *et al.*, 1998; Garzanti, 1999), whereas the northern Tethyan Himalaya is dominated by Mesozoic to Palaeogene deep-water outer shelf, continental slope and rise deposits (Liu & Einsele, 1994; Hu *et al.*, 2008). This study focuses on the Upper Cretaceous–Palaeogene strata exposed at the Zhepure Mountain of southern Tibet, which belong to the southern Tethyan Himalaya, and is located about 60 km south of the Indus-Yarlung suture zone (Fig. 1a).

During Jurassic-Early Cretaceous time, the northern margin of Greater India was situated at high-to-middle latitudes in the southern hemisphere (Patzelt *et al.*, 1996), while the Lhasa block was in low latitudes of the northern hemisphere (Achache *et al.*, 1984). The Neo-Tethyan ocean separated Greater India from the Lhasa block, and must have been thousands of kilometres wide during this period (see review by Ali & Aitchison, 2008). Greater India rifted from the Australian-Antarctic continent in Early Cretaceous time (Zhu *et al.*, 2009a), started to drift northward in late Early Cretaceous time (Gaetani & Garzanti, 1991; Hu *et al.*, 2010) and collided with the Lhasa block (Asian plate) sometime between latest Cretaceous and Eocene time.

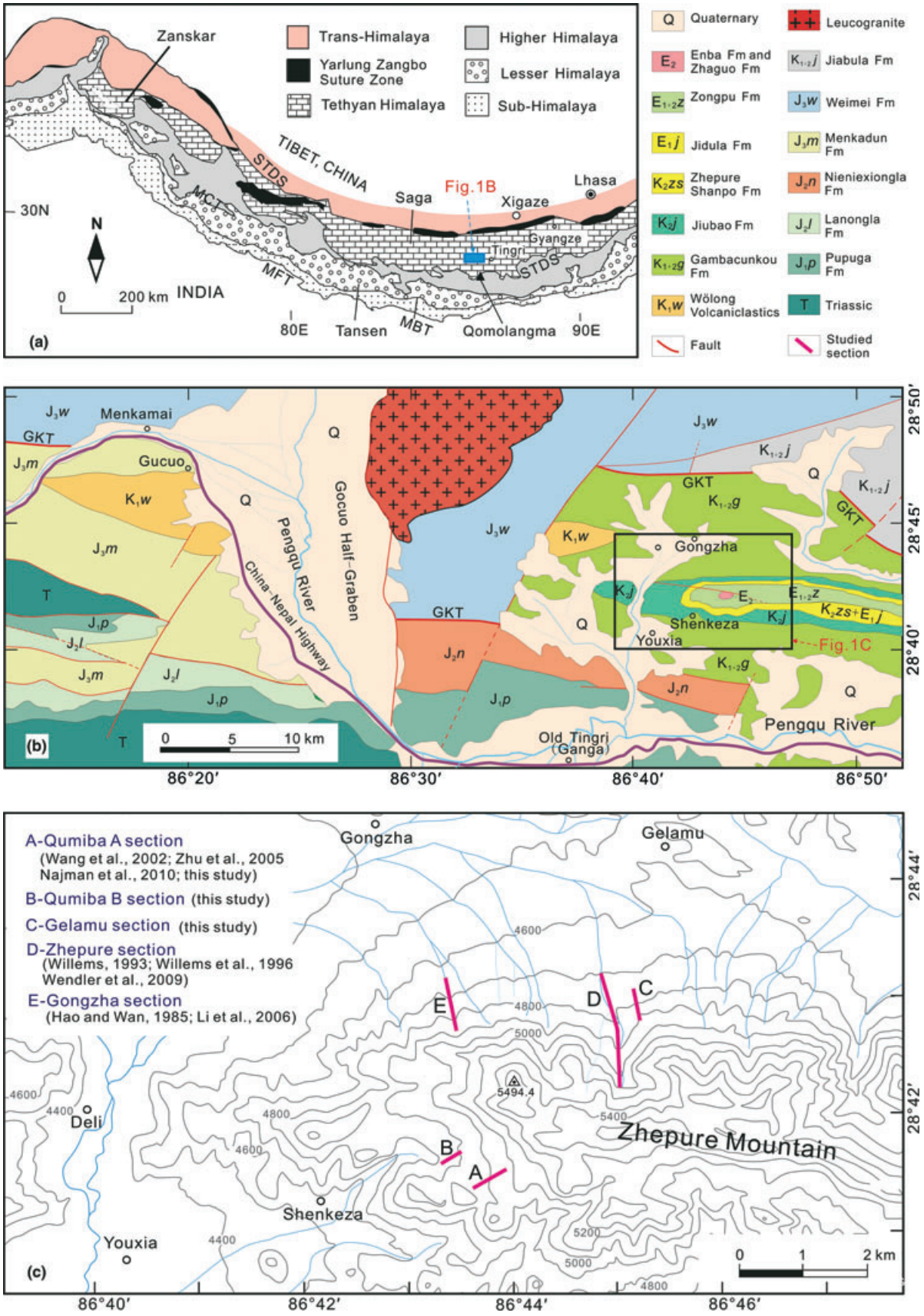

Fig. 1. (a) Geological sketch map of the Himalayas, modified from Gansser (1964). MFT: Main Front Trust; MBT: Main Boundary Trust; MCT: Main Central Trust; STDS: South Tibetan Detachment System. (b) Geological map of the western part of the Zhepure Mountain revised after Zhu *et al.* (2002). GKT: Gyirong–Kangmar Thrust. (c) Topographical map of the studying area in the Zhepure Mountain showing the stratigraphic sections from previous studies and from this work.

STRATIGRAPHY AND SEDIMENTOLOGY

The Zhepure Mountain area is a type locality for Upper Cretaceous to Palaeogene stratigraphy in the southern Tethyan Himalaya (Heron, 1922; Mu *et al.*, 1973; Hao & Wan, 1985; Willems & Zhang, 1993; Willems *et al.*, 1996; Wang *et al.*, 2002a; Zhu *et al.*, 2005; Li *et al.*, 2006; Wendler *et al.*, 2009; Najman *et al.*, 2010) (Fig. 1b, c; Table 1). Most studies have focused on the northern side of the Zhepure Mountain, such as the Zhepure section of Willems *et al.* (1996), and the Gongzha section of Hao & Wan (1985) and Li *et al.* (2006) (Fig. 1c). Our study focuses on the southern slopes of the Zhepure Mountain.

Summary of lithostratigraphy and palaeo-environments

In the Zhepure section (Fig. 1c), the Gambacunkou Formation (Fig. 2) consists of a monotonous, *ca.* 600 m thick succession of grey calcareous marlstones and marly limestones with abundant planktonic foraminifera (Willems *et al.*, 1996; Li *et al.*, 2006; Wendler *et al.*, 2009). The overlying Jiubao Formation (Zhepure Shanbei Formation of Willems *et al.*, 1996), is approximately 80 m thick, and dominated by regular bedded limestone with abundant planktonic foraminifera (Wendler *et al.*, 2009). The ages of the Gambacunkou Formation and Jiubao Formation were well dated by planktonic foraminifera as late Albian–early Coniacian and early Coniacian to latest Santonian, respectively (Willems *et al.*, 1996; Wendler *et al.*, 2009). The Gambacunkou and Jiubao formations have been interpreted as having accumulated in hemi-pelagic and pelagic, outer shelf environment (Willems, 1993; Willems *et al.*, 1996).

The overlying Zhepure Shanpo Formation (*ca.* 190 m thick; Figs 3 and 4) is characterized by mixed siliciclastic – carbonate rocks (Willems *et al.*, 1996; Wan *et al.*, 2002). The siliciclastic sandstones are interpreted as turbidites becoming increasingly sandstone-rich up the section (Willems & Zhang, 1993). The sedimentary development of the Zhepure Shanpo Formation has been interpreted as recording a transition from distal continental slope in the lower part, to a proximal continental slope turbidite fan in the upper part of the formation, representing an overall shallowing upward sequence (Willems *et al.*, 1996; Fig. 2). The lower part of the Zhepure Shanpo Formation is latest Campanian to Maastrichtian in age based on planktonic foraminifera (Willems *et al.*, 1996; Fig. S3). In the uppermost part, planktonic foraminifera, benthic foraminifera and ostracodes indicate an early Danian age (Wan *et al.*, 2002).

The 75-m-thick Jidula Formation (Willems *et al.*, 1996; Wan *et al.*, 2002) comprises mainly calcareous quartz sandstones, with one layer of about 15-m thick of shales in the middle. The uppermost part of the Jidula Formation is composed of 13 m of nodular, fossiliferous marly limestones. Few fossils were reported in the Jidula Formation, including foraminifera: *Lenticulina* sp., *Oolina*

Table 1. Stratigraphic summaries on the Cretaceous–Palaeogene strata in the Zhepure Mountain, southern Tibet, and the palaeo-water depth with bathymetric error used for subsidence analysis.

Age (stages)	Ma	Formation	Other names with references*	Thickness (m)	Palaeo-water depth (m)	Palaeo-water depth error (m)	References*
Palaeogene younger than middle Lutetian	<43 or <35	Zhaguo	Pengqu (1); Shenkeza (3)	75	Nonmarine		1, 2, 3, 4
Ypresian	51–49	Enba	Youxia (3)	105	50–150	50	1, 2, 3, 4
Late Danian – Ypresian	62–51	Zongpu	Zhepure Shan (1)	350–440	0–50	20	1, 5, 6
Early Danian	64–62	Jidula		75	200–0	50	1, 5
Late Campanian- early Danian	72–64	Zhepure Shanpo		190	400–200	100–50	1
Cretaceous							
Early Coniacian – earliest Campanian	88–83	Jiubao	Zhepure Shanbei (1); Zongshan (5)	80	300–400	100	1, 5, 7
Late Albian-early Coniacian	100–88	Gangbacunkou		600	200–300	50–100	1, 7, 8

*1: Willems *et al.*, 1996; 2: Wang *et al.*, 2002a; 3: Zhu *et al.*, 2005; 4: Najman *et al.*, 2010; 5: Hao & Wan, 1985; 6: Wan *et al.*, 2002; 7: Li *et al.*, 2006; 8: Wendler *et al.*, 2009.

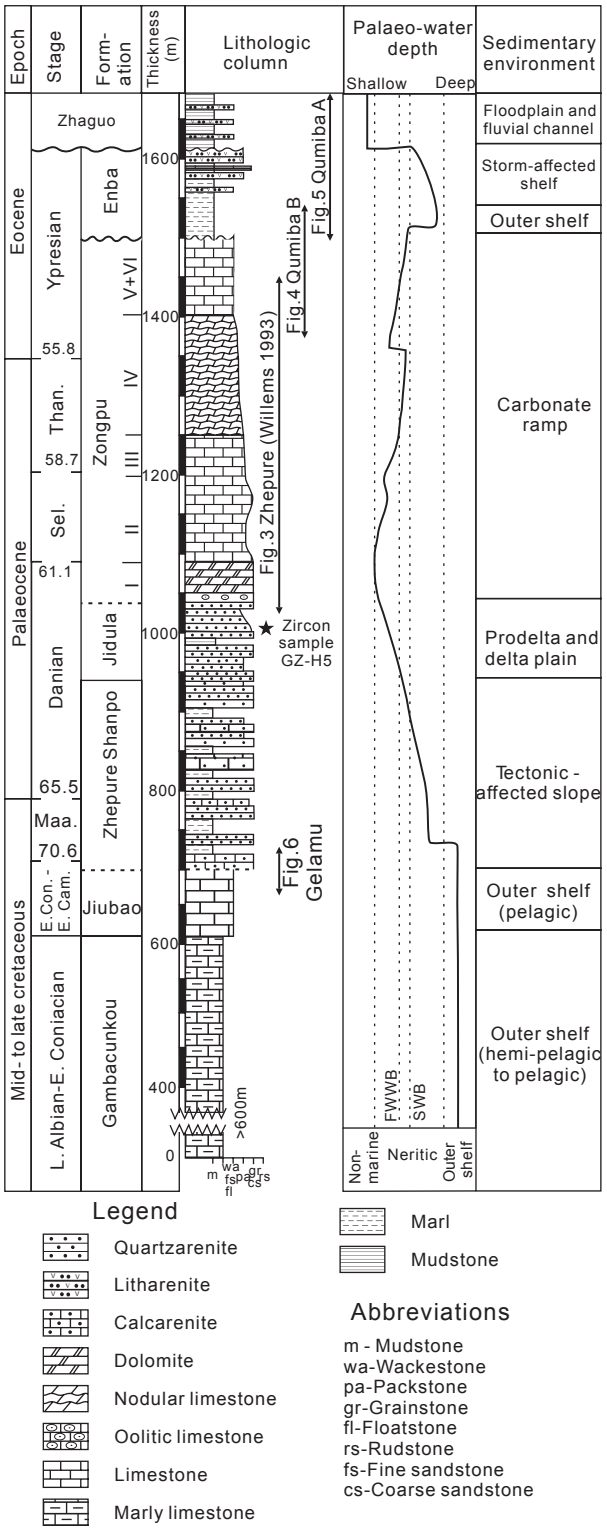

Fig. 2. Composite stratigraphic log of the Cretaceous – Palaeogene strata at the Zhepure Mountain area showing interpreted palaeo-water depth trend and sedimentary environments. Subsequent figures are also located. Stratigraphy is mainly adapted from Hao & Wan (1985); Willems *et al.* (1996), and Wang *et al.* (2002a). FWWB–fare weather wave base; SWB–storm wave base.

sp., *Morozovella* sp. and ostracods *Bairdia* sp indicating a likely early Danian age (Wan *et al.*, 2002). The depositional environment of the Jidula Formation is interpreted as a prodelta environment in the lower part and a prograding delta plain in the upper part (Willems, 1993). Thus, the sandstones of the Jidula Formation represent a continuation of the overall shallowing upward trend, as already indicated by the sedimentary development of the underlying Zhepure Shanpo Formation.

The Jidula Formation is overlain by the Zongpu Formation (Hao & Wan, 1985; equal to the Zhepure Shan Formation of Willems *et al.*, 1996), but the contact is not exposed. The Zongpu Formation is 350- to 440-m thick, and comprises thick-bedded to massive limestones, selectively dolomitized at the basal part, nodular limestones in the middle part of the formation, and thick-bedded, large benthic foraminifera-bearing limestones in the upper part (Hao & Wan, 1985; Willems & Zhang, 1993; Willems *et al.*, 1996) (Fig. 2).

Willems (1993) studied the Zongpu Formation in the Zhepure section (Fig. 1c) and recognized 12 microfacies (Fig. 3; Table S1) that record the transition from intertidal ooid shoals to shallow subtidal nearshore environments that contain numerous large benthic foraminifera. Overall, the succession records a deepening trend of sea level change up-section (Fig. 3). The age of the Zongpu Formation at this section can be defined by planktonic and large benthic foraminifera. In the lower part of the Zongpu Formation, Wan *et al.* (2002) found abundant foraminifera which indicate a late Danian (*ca.* 62 Ma) up to Thanetian age. Near the top of the Zongpu Formation, microfossils including large benthic foraminifera indicate an early Eocene age (Ypresian substage, shallow benthic zone SBZ 8, *ca.* 53–54 Ma; planktonic foraminifera zone lowermost P7/P6, *ca.* 54.5–52.5) (Zhu *et al.*, 2005; Najman *et al.*, 2010).

A suite of sandstones and shales stratigraphically overlying the Zongpu Formation was discovered at the Qumiba A section (Fig. 1c, GPS N28°41′26.3″, E86°43′38.7″, elevation 4966 m; Wang *et al.*, 2002a; Zhu *et al.*, 2005; Najman *et al.*, 2010). Wang *et al.* (2002a) named this sequence the Pengqu Formation and subdivided it into a lower, green-coloured Enba member and an upper red-coloured Zhaguo member. We retain Enba and Zhaguo names here, but reclassify the members as formations, considering the angular unconformity contact between the two (see below). The Enba Formation comprises approximately 105 m of greenish-grey shale intercalated with thin-bedded, green-coloured sandstones and rare thin nodular limestone beds (Fig. 5). Detrital modes of the sandstones in the Enba Formation show that they are mainly litharenites with significant volcanic fragments (Zhu *et al.*, 2005). The age of the Enba Formation was constrained by planktonic foraminifera as zone P8 by Zhu *et al.* (2005); 50.5 Ma, Ypresian of the time scale of Gradstein *et al.*, 2004) and youngest calcareous nannofossils of the NP11–12 (Ypresian, 50.6–52.8 Ma, Najman *et al.*, 2010).

The Zhaguo Formation is about 75-m thick in the Qumiba A section (Fig. 1c), and consists of red mudstone and lenses of sandstone (Fig. 5) that have the sedimento-

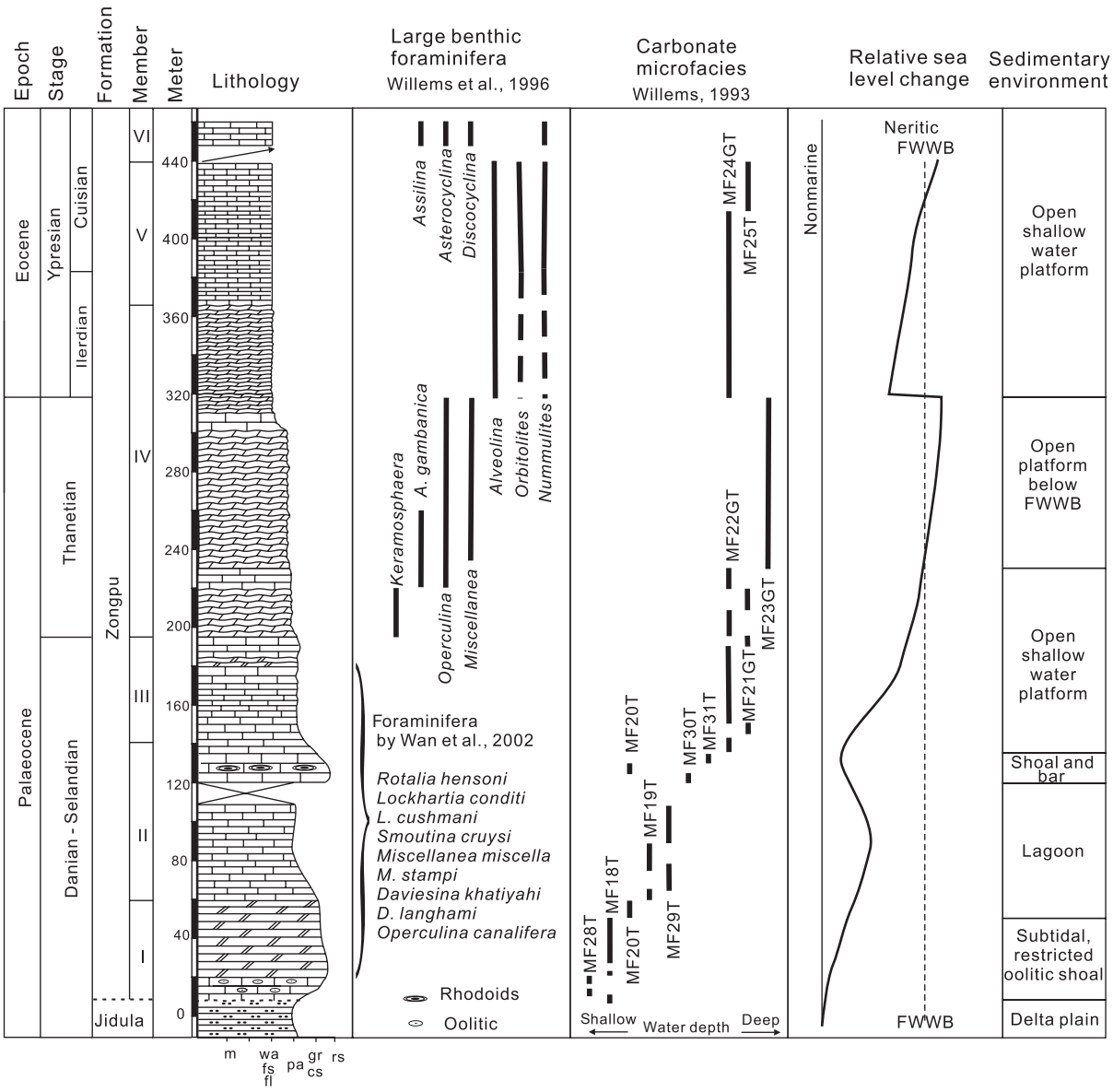

Fig. 3. Lithological log of the Zongpu Formation at the Zhepure section showing distribution of large benthic foraminifera (Willems *et al.*, 1996; Wan *et al.*, 2002), carbonate microfacies (Willems, 1993) and interpreted palaeo-water depth and sedimentary environment. Legend refers to Fig. 2.

logical characteristics of fluvial channel and floodplain deposits as suggested by Zhu *et al.* (2005). The boundary between the green arenites of the Enba Formation and red shales of the Zhaguo Formation is marked by a 25-cm-thick bed of poorly sorted, angular, pebble/cobble-sized material derived from the underlying unit which was interpreted as a palaeoregolith (Zhu *et al.*, 2005). Detrital modes of the sandstones in the Zhaguo Formation (Zhu *et al.*, 2005) are very similar to those of Enba Formation. The age of the Zhaguo Formation remains disputed. Both Wang *et al.* (2002a) and Najman *et al.* (2010) found stratigraphically mixed nannofossils assemblages of Mesozoic – Palaeogene pollens. The youngest nannofossils were assigned to a nannofossil zone NP20, at approximately *ca.* 35 Ma by Wang *et al.* (2002a). However, Najman *et al.* (2010) found no difference between the calcareous nannofossil assemblages preserved in the Enba and Zhaguo formations, with the youngest fauna belonging to the nannofossil zone NP11-12 (Ypresian, 50.6–53.5 Ma).

Further stratigraphic and sedimentary analysis

Zhepure Shanpo formation

In the Gelamu section (Fig. 1c, GPS N28°42′47.9″, E86°45′13.4″, elevation 4883 m), about 500 m east of the Zhepure section of Willems *et al.* (1996), we recognized a disconformity within the upper part of the Jiubao (Zhepure Shanbei) Formation of Willems *et al.* (1996) (Fig. 6a). Above the boundary are *ca.* 25 m of medium-

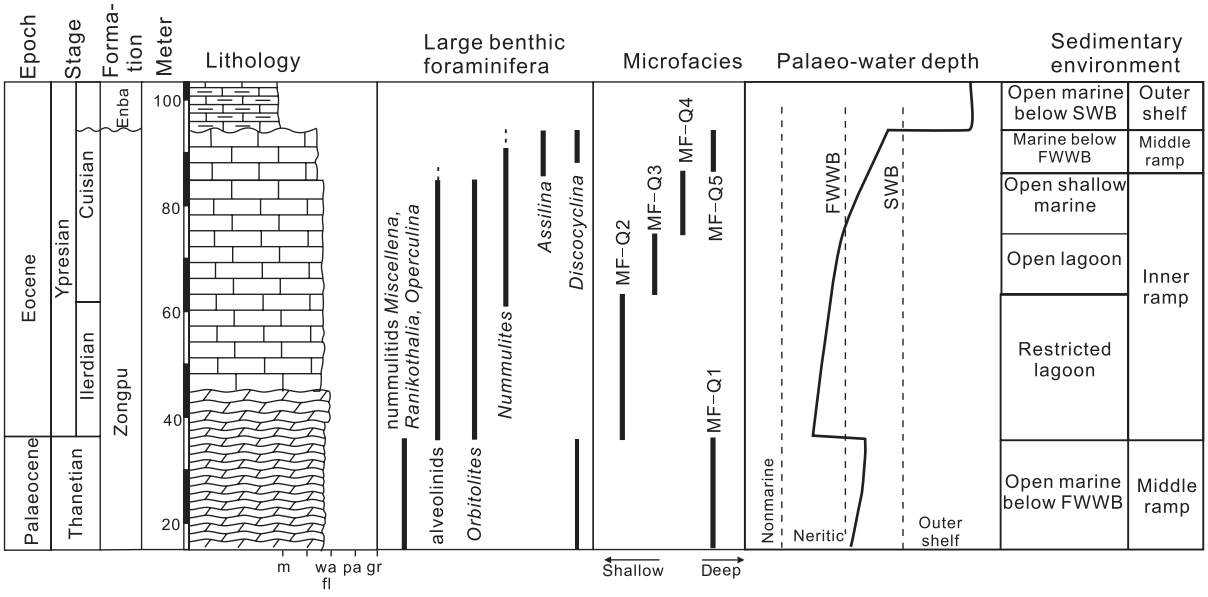

Fig. 4. Lithological log of the upper part of the Zongpu Formation at the Qumiba B section showing distributions of large benthic foraminifera, carbonate microfacies, and interpreted palaeo-water depth and sedimentary environment. Legend refers to Fig. 2.

bedded limestones (mainly packstones and grainstones, Fig. 6b) with abundant planktonic foraminifera and calcispheres. The limestone beds are irregular, sometimes lenticular and discontinuous along strike (Fig. 6d). The beds exhibit (1) many planktonic foraminifera that show reworking recorded by broken fragments in the thin sections; (2) mixed foraminifera from different foraminiferal zones and different ages located along the same horizon; (3) biota of pelagic and neritic origin; and (4) limestones characterized by high quantities of reworked calcareous intraclasts of a shallow-water facies with large benthic fossils (Willems *et al.*, 1996). On the basis of these observations, we interpret these beds as calciturbidites which should be grouped into the Zhepure Shanpo Formation, instead of the Jiubao Formation (Zhepure Shanbei Formation) of Willems *et al.* (1996).

The uppermost of Jiubao Formation (Fig. 6c) was dated by the planktonic foraminifera *D. asymetrica* Zone (Willems *et al.*, 1996; Wendler *et al.*, 2009), which can be extended into latest Santonian (*ca.* 84 Ma; Wu *et al.*, 2011; Fig. S3). The youngest planktonic foraminifera in the lowermost part of the Zhepure Shanpo Formation indicate an age of latest Campanian (*ca.* 72 Ma according to Wu *et al.*, 2011; see Fig. S3). Thus, most of the Campanian period is missing across the disconformity between these two formations.

Zongpu formation

In the Qumiba B section (Fig. 1c, GPS N28°41′37.4″, E86°43′23.4″, elevation 4884 m), we studied the upper part (about 80 m) of the Zongpu Formation. Five microfacies can be recognized from bottom to top (Fig. 4; Table S1):

MF-Q1, Floatstone with nummulitids (Fig. S1A). Large benthic foraminifera (30–60%) are mainly represented by *Miscellanea* and *Ranikothalia*. In the upper level occur *Discocyclina, Operculina, Keramosphaer*. Debris of *Dasycladacean* algae (10–20% in content) occur. The matrix is micritic. The environment of this facies is interpreted as open marine below fair weather wave base.

MF-Q2, Floatstone with alveolinids (Fig. S1B). Large benthic foraminifera are alveolinids (mainly *Glomoalveolina* in the lower part, with increasing *Alveolina* upward, which become dominant in the upper part). Small benthic foraminifera are abundant (20–30% in content), and consist mainly of rotaliids and miliolids. The contents of red algae (mainly *Lithoporella)* may be up to 10%. Occasionally, echinoderms debris occur up to 10% in content. The matrix is mainly micritic, although, in some parts, sparites are present. The environment is interpreted as restricted marine, possibly lagoonal.

MF-Q3, Floatstone with *Alveolina* and *Nummulites* (Fig. S1C). Large benthic foraminifera comprise 20–45% in content mainly *Alveolina* with minor *Nummulites*. Small benthic foraminifera comprise 15–30%, and are mainly rotaliids and miliolids. Debris of *Dasycladacean* algae comprise 5–20% in content. The matrix is micritic, with occasional sparites in the lower part. The environment is interpreted as restricted, possibly lagoonal.

MF-Q4, Floatstone with *Nummulites* and *Alveolina* (Fig. S1D). Large benthic foraminifera comprise 25–45% in content, mainly *Nummulites* with minor *Alveolina*. Small benthic foraminifera comprise 5–30% in content, mainly rotaliids and miliolids, which decrease up-section. Planktonic foraminifera occur 5–10% in content and increase up-section. Matrix is micritic. The environment of this facies is interpreted as open shallow marine.

MF-Q5, Floatstone/rudstone with *Assilina* and *Discocyclina* (Fig. 7b; Figs S1E and S1F). The composition is mainly floatstones with some rudstones. Large benthic

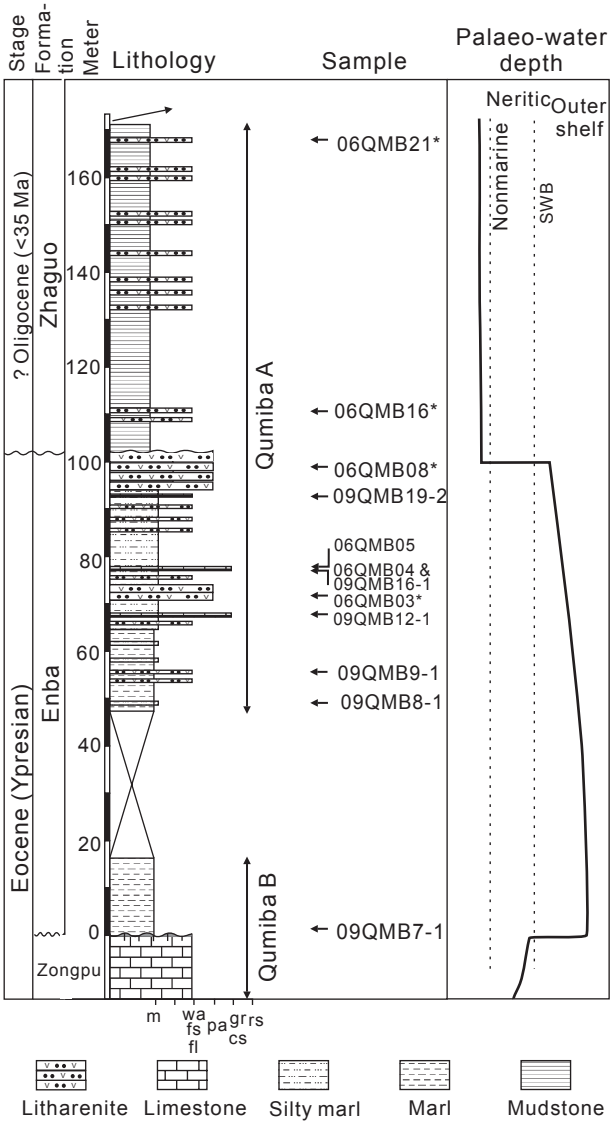

Fig. 5. Lithological log of the Enba and Zhaguo formations at the Qumiba A section showing interpreted palaeo-water depth and studied samples of thin sections. Samples with star (*) are analysed detrital zircon samples. Legend refers to Fig. 2.

foraminifera are 40–70% in content, mainly *Assilina, Discocyclina,* minor *Nummulites, Asterocyclina*. Small benthic foraminifera are 5–30% in content, mainly rotaliids and miliolids. Planktonic foraminifera may reach up to 15% in content. Red algae (3–10% in content) occur. The matrix is micritic. The environment of this facies may be relatively deep-water below the influence of wave action on the sea-floor, which was supported by the co-occurrence of planktonic foraminifera and flat large benthic foraminifera (*Discocyclina* and *Assilina*).

An abrupt turnover of large benthic foraminifera occurred within the nodular limestones in the lower part of this section (Fig. 4). The large benthic foraminifera of *Miscellanea*, *Ranikothalia*, *Operculina* and *Discocyclina* of Thanetian age in underlying strata disappeared and are replaced by *Alveolina*, *Orbitolites* and *Nummulites* of Ypresian age, representing the Palaeogene–Eocene boundary. This biotic boundary is associated with an abrupt shallowing palaeoenvironmental change from open marine below wave influence (microfacies MF-Q1) to lagoon or restricted sea (microfacies MF-Q2) (Fig. 4). Starting from the Palaeogene–Eocene boundary up to the top of the formation, the strata represent a deepening water-depth trend (Fig. 4).

Enba formation

The contact between the Zongpu Formation and Enba Formation was thought to be conformable according to Wang *et al.* (2002a) and Zhu *et al.* (2005). However, in the Qumiba B section (Fig. 1c), on the top of the Zongpu Formation (Fig. 7b), some beds of limestones are truncated by the Enba Formation (Fig. 7a). Therefore, a slight angular unconformity is suggested to separate the Enba Formation from the underlying Zongpu Formation.

In the Qumiba A and B sections, the Enba Formation can be further divided into two parts. The lower part (*ca.* 30 m) of the Enba Formation is mainly composed of grey calcareous hemipelagic marls (Figs 5 and 7d) with planktonic foraminifera, without any sandstones beds. The environment of deposition is interpreted to have been relatively deep-water outer shelf, below the influence of wave activity. The upper part of the Enba Formation is about 50 m thick and mainly composed of calcareous shales interbedded with thin-to-thick bedded lithic arenites (Fig. 5). Sandstone beds have tabular geometries and become more numerous, thicker, and coarser grained up-section. Bed thickness of sandstones varies from a few centimetres up to one metre. Abundant bioturbation is present on the top surfaces of some sandstones beds. Some are normally graded with widespread planar and ripple cross-lamination. Near the top is undulatory laminated bedding that may represent hummocky cross-stratification (Fig. 7c). Some sandstone beds have scoured bases that display tool marks. Several oolitic limestones (Fig. S1G) and shell-rich bioclastic limestones (Fig. S1H) were found in this middle part of the Enba Formation. Both ooids and mixed bioclastic debris are reworked together with terrigenous materials, interpreted as storm beds. Thus, the environment of deposition for the upper part of the Enba Formation is interpreted as a storm-affected outer shelf.

Zhaguo formation

The boundary between the Enba and Zhaguo formations within the Qumiba B section is a slight angular unconformity with <15° of discordance (Fig. 7e). The red shales of the lowermost part of the Zhaguo Formation contain green mottles and angular/blocky pedogenic structures. Sandstone beds have lenticular geometries, are commonly 1–3 m in thickness and tens to hundreds of metres in width (Fig. 7f). Individual sandstone beds have scoured bases, fine upward, and contain trough cross-stratification, horizontal lamination, and ripple cross-lamination. We

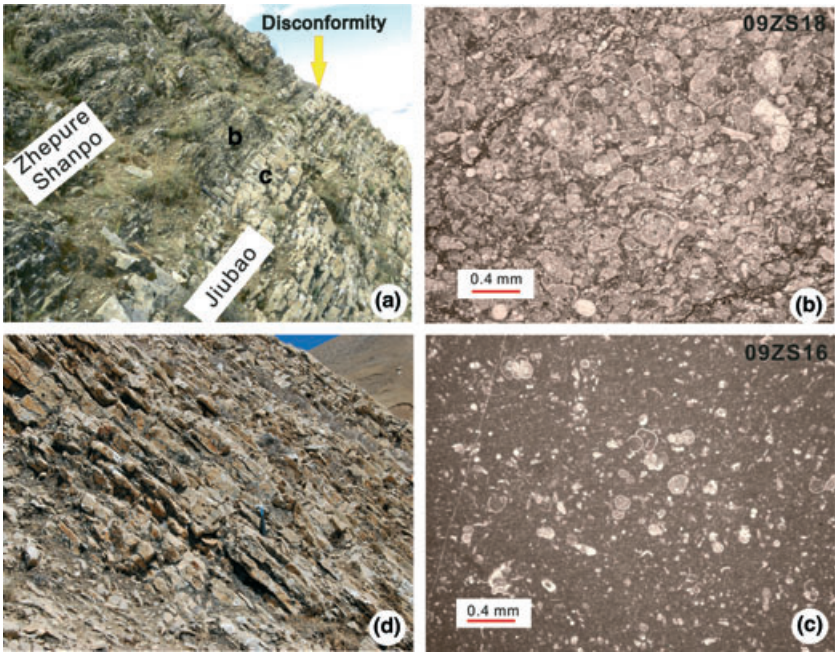

Fig. 6. (a) Field photograph showing the disconformity between the Jiubao Formation and overlying Zhepure Shanpo Formation. (b) Calciturbuditic grainstone with redeposited planktonic foraminifera, sample 09ZS18 from the lowermost Zhepure Shanpo Formation. (c) Wackestone with planktonic foraminifera, Sample 09ZS16 from the uppermost Jiubao Formation. (d) Detail of the limestone sequence of the lower part of the Zhepure Shanpo Formation showing unevenly bedded banking structure. These limestones are interpreted as calciturbuditic origin.

interpret the sedimentary environment of the reddish Zhaguo Formation as fluvial channel and floodplain deposits as suggested by Zhu *et al.* (2005). We suggest that all the marine fossils found from the Zhaguo Formation were reworked from underlying strata, probably the Enba Formation; this is supported by the slight angular discordance and provenance data (see below).

Summary of palaeo-water depth trends

Following the sustained deep-water conditions recorded by the Gambacunkou and Jiubao Formations, the Zhepure Shanpo and Jidula formations record an abrupt transition into an overall shallowing-upward trend from distal continental slope in the lower part, a proximal continental slope turbiditic fan in the upper part of the Zhepure Shanpo Formation, to prodelta – delta plain environment of the Jidula Formation (Willems, 1993) (Fig. 2).

Microfacies reveal two deepening successions of a carbonate ramp setting in the Zongpu Formation (Figs 3 and 4). The first deepening trend recorded in the Zhepure section (Willems, 1993) extends from the bottom of the formation to the upper part of Member IV of the Zongpu Formation: starting in high-energy shoals with ooid bars at the lower part, low-energy protecting lagoonal areas, high-energy rhodolid bars and shoals in the middle, slowly changing into to open marine below wave base near the top (Fig. 3). The second deepening trend starts at around the Palaeocene/Eocene boundary with deposits of a restricted lagoon setting, which were recorded both in the Zhepure section and the Qumiba B section (Figs 3 and 4). Up-section, it changes into shallow marine and finally open marine environments below wave base near the top of the Zongpu Formation in the Qumiba B section (Fig. 4).

The boundary between the Zongpu Formation and the Enba Formation represents the drowning surface of the Zongpu carbonate platform. The lower part of the Enba Formation was deposited in a hemi-pelagic, relatively deep-water environment below storm wave base. The upper part of Enba Formation shows a shallowing trend up-section, and is interpreted to be deposited in a storm-affected outer shelf environment. Finally, there is an abrupt shallowing across the boundary between the Enba and Zhaguo formations as the system records fully non-marine sedimentation.

SUBSIDENCE ANALYSIS

Subsidence analysis was performed on 1455 m of the Cretaceous-Eocene strata in Zhepure Mountain starting from the base of the Gambacunkou Formation (*ca.* 100 Ma) to the unconformity at the top of the Enba Formation at around *ca.* 50 Ma (Table 1). The analysis was run using the MATLAB code provided online from Allen & Allen (2005). Each formation was decompacted and then sequentially recompacted during progressive burial by the overlying succession. The succession was then backstripped to remove the effects of sediment loading; these calculations assumed an Airy isostatic correction. Calculations using possible values for the effective elastic

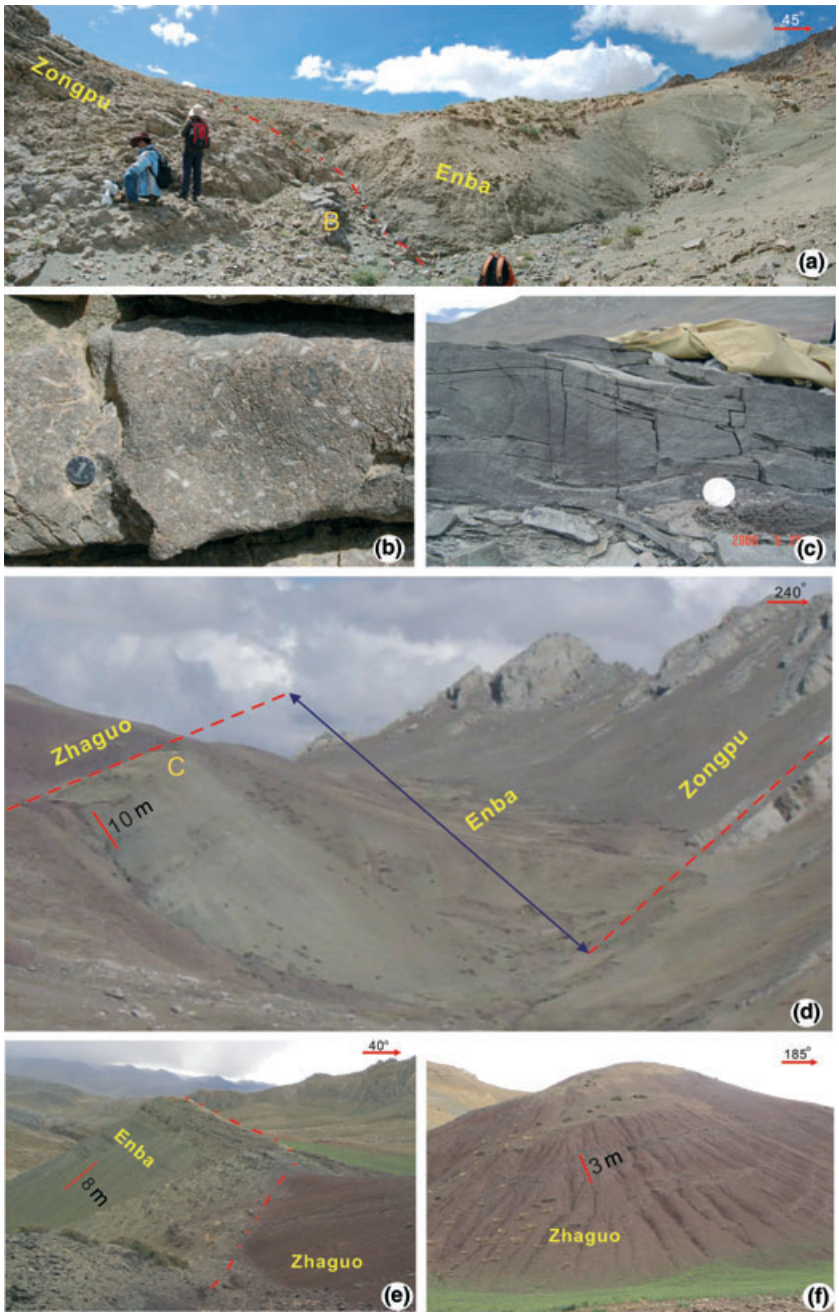

Fig. 7. (a) Field photograph showing a disconformity between the Zongpu Formation and overlying Enba Formation; Stand -up person (*ca.* 1.6 m) as scale. The position of the Fig. 7b is indicated. (b) Field photograph from uppermost Zongpu Formation, showing abundant large benthic foraminifera. (c) Hummocky cross-stratification, uppermost part of the Enba Formation; Coin as scale. (d) Photograph showing outcrops at the Qumiba A section, viewed towards the northeast. From right to left, the sedimentary sequences are: the massive Zhepure Formation limestone; the greyish Enba Formation and the violet-reddish Zhaguo Formation. The position of the Fig. 7c is indicated. (e) photograph showing the contact between the Enba and Zhaguo formations. (f) photograph showing the overview of the Zhaguo Formation. Lens of sandstones are visible.

strength of the Indian passive margin would reduce the correction, and hence yield greater values for the total tectonically forced subsidence. However, without constraint on the strength of the plate during this period, and with the primary concern here being the signal of subsidence rather than the absolute values, it was chosen to assume local compensation of the sediment load. For all calculations, values for the initial porosity, the exponents describing the loss of porosity with burial and sediment densities were taken from comparable lithologies listed in Allen & Allen (2005).

The final step in the derivation of the tectonic subsidence history required a correction for palaeobathymetry of the succession, and for any eustatic signal. The palaeobathymetry values are based on the sedimentological and palaeontological analyses summarized above and incorpo-

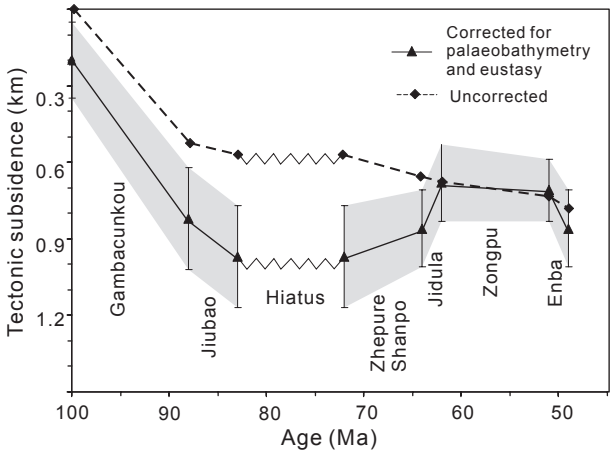

Fig. 8. Subsidence curves generated from two sections in the Zhepure Mountain including the Qumiba and Gelamu sections located in Fig. 1. The data used for these calculations is listed in Table 1. The calculations are based on the MATLAB code provided online by Allen & Allen (2005). The dashed curve with diamonds is the tectonic subsidence curve uncorrected for palaeobathymetry and eustasy (from Kominz *et al.*, 2008). The corrected curve is shown in a solid line with shading reflecting error estimates on the palaeobathymetry. For discussion, see text.

rate error bars. Prior to this correction, the cumulative tectonic subsidence was *ca.* 780 m. Therefore, with the water depths ranging from outer shelf, hemipelagic settings to lagoonal, this correction plays a major role in the derived tectonic subsidence plot (Fig. 8). The corrections for eustasy through this period will vary depending on the derived curve that is chosen. For this, we have used Kominz *et al.* (2008) as this is the most recent analysis. We have used the first-order signal of eustatic change yielding no change through most of the period 100 to *ca.* 60 Ma, but then a higher value of approximately 70 m for the period *ca.* 55–40 Ma. Hence, we have applied this correction to the youngest two values in the curve (Fig. 8).

The fully corrected subsidence curve suggests steady tectonic subsidence during accumulation of the Gambacunkou and Jiubao formations followed by a hiatus until *ca.* 72 Ma. The Zhepure Shanpo and Jidula formations are thought to have accumulated in a submarine setting while the basement was being actively uplifted by approximately 300 m (±200 m) over 10 Myr; the large errors reflect uncertainty in palaeobathymetric values. The Zhepure Shanpo Formation then records stability with no subsidence followed by renewed subsidence during accumulation of the Enba Formation. As stated, there are large errors on these calculations, and so absolute values are likely to vary, but the overall signal of subsidence, uplift, stability and renewed subsidence is the most probable solution for the data.

SANDSTONE PROVENANCE ANALYSIS

Previous studies (Wang *et al.*, 2002a; Zhu *et al.*, 2005; Najman *et al.*, 2010) suggested that the Enba and Zhaguo formations show the first evidence of erosion of ophiolites and continental arc rocks of the Asian margin based on the presence of volcanic lithic fragments, chemical composition of Cr-spinel and geochemistry of siliciclastic rocks. However, Aitchison *et al.* (2007) proposed that the sedimentary detritus may have been derived from an intraoceanic arc and ophiolite sequence, the combined Dazhuqu-Baingang-Zedong terranes, remnants of which are exposed along the Indus-Yarlung suture zone. Recently, Najman *et al.* (2010) challenged this interpretation using detrital zircon U–Pb dating. However, the dataset of Najman *et al.* (2010) comprised only 20 grains of detrital zircons in the Enba Formation and 16 grains in the Zhaguo Formation. To clarify the sources for these successions, we carried out combined detrital zircon U–Pb dating and Hf isotopes through the entire succession.

Samples and methods

Five sandstone samples from different stratigraphic levels at the Zhepure Mountain were analysed for sediment provenance (Figs 2 and 5) through detrital zircon U–Pb–Hf isotopic study. Sample GZ-H5 is a quartz arenite, sampled from the uppermost part of the Jidula Formation at the Gelamu section. Samples QMB03 and QMB08 are lithic arenites collected from the Enba Formation, whereas samples QMB16 and QMB21 are lithic arenites collected from the Zhaguo Formation (Fig. 5) at the Qumiba A section.

Zircon grains from the Enba Formation are angular to sub-angular and small, with most of the grains about 30–50 μm in diameter. Zircons from the Zhaguo Formation are angular to sub-angular and mostly 50–80 μm in diameter. Zircon grain shape was documented by micrographs and backscattered electron images.

U–Pb dating and Hf isotope analysis were conducted at the Institute of Geology and Geophysics, CAS, China and the GEMOC, Macquarie University, Australia, except for some zircon U–Pb dating that was carried out at the State Key Laboratory for Mineral Deposits Research, Nanjing University, China.

U–Pb isotopic measurements were performed by laser ablation inductively coupled plasma mass spectrometry (LA–ICP–MS), using a spot diameter of 20, 25 or 30 μm depending on zircon grain size following the method described by Jackson *et al.* (2004). Most zircons are concordant in terms of detrital zircon U–Pb ages (see Fig. S2). Results described in this article exclude analyses with $\geq 20\%$ discordance. Zircon age interpretations are based on $^{206}Pb/^{238}U$ ages for grains less than 1000 Ma and $^{207}Pb/^{206}Pb$ ages for grains greater than 1000 Ma. All ages are interpreted according to the geological time scale of Gradstein *et al.* (2004).

Younger U–Pb age zircons (<250 Ma) were selected for Lu–Hf isotope analyses, using a Nu Plasma MC ICP–MS with Merchantek/NWR 213 mm laser-ablation microprobe in GEOMOC, Macquarie University, Australia, and a Neptune with a Geo plus 193 nm laser at the Institute of Geology and Geophysics, CAS, following the

procedure described by Griffin *et al.* (2000). To calculate model ages (T_{DM}) and epsilon Hf, we have adopted the depleted mantle with $^{176}Hf/^{177}Hf = 0.28325$ and $^{176}Lu/^{177}Hf = 0.0384$ and chondrite with $^{176}Hf/^{177}Hf = 0.282772$ and $^{176}Lu/^{177}Hf = 0.0332$ (Griffin *et al.*, 2000). The decay constant of ^{176}Lu adopted in this paper is 1.867×10^{-11} yr^{-1} (Soederlund *et al.*, 2004).

Detrital zircon U–Pb ages

Seventy-three zircon grains from sample GZ-H5 (Jidula Formation) (Table S2) show a significant peak of Early Cretaceous zircons, with ages ranging from 109 to 145 Ma (n = 20; Fig. 9). Another zircon age cluster occurs in the Cambrian, with zircon ages ranging from 482 to 572 Ma (n = 11; Fig. 9). These two age peaks are characteristic of those commonly found in Tethyan Himalayas sequences (Gehrels *et al.*, 2003; Cawood *et al.*, 2007; Hu *et al.*, 2010). Precambrian-age zircons mostly comprise a wide age group between 807 and 1417 Ma, with small clusters at *ca.* 1650–1850, *ca.* 2000–2500 and *ca.* 3250–3350 Ma (Fig. 9).

One hundred and twenty-one grains of 203 accepted detrital zircons with an age <250 Ma from the Enba Formation (samples QMB03 and QMB08) have a prominent age peak between 80 and 103 Ma (55 grains) and a subordinate peak between 52 and 70 Ma (24 grains; Fig. 9). A third cluster of 21 grains occurs at 108–143 Ma. There is a small group of zircons with ages ranging from 179 to 226 Ma, and an additional two grains with ages of 241–242 Ma.

One hundred and forty-nine grains of 238 accepted detrital zircons with an age <250 Ma from the Zhaguo Formation (samples QMB16 and QMB21) show a similar age pattern when compared with the underlying Enba Formation, and are characterized by a prominent peak at 79–108 Ma (69 grains) and two subordinate peaks at 52–73 Ma (32 grains) and 111–140 Ma (22 grains; Fig. 9). The Zhaguo Formation also contains three small groups of zircons that range in age from 181 to 218 Ma (13 grains), 150–169 (six grains) and 236–241 Ma (three grains; Fig. 9).

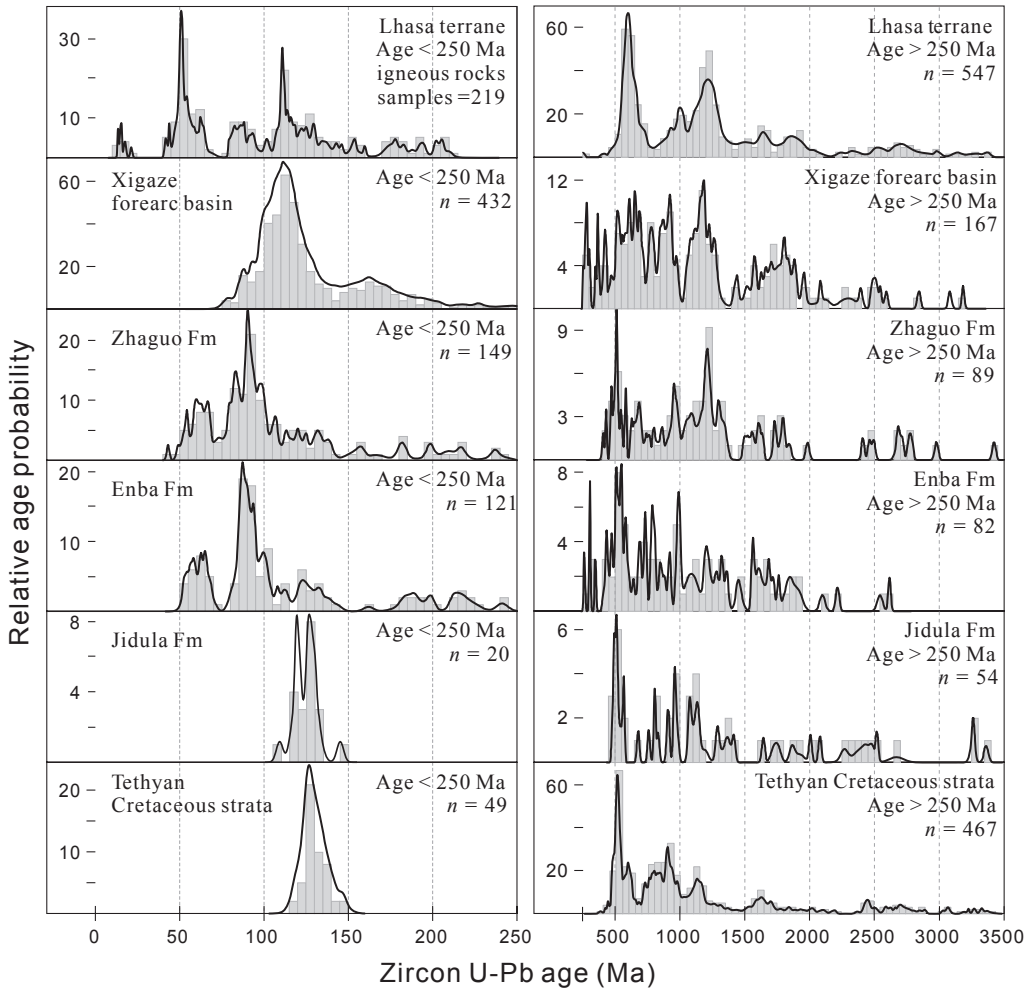

Fig. 9. Relative probability plots of analysed U-Pb data. Zircon ages are $^{207}Pb/^{206}Pb$ ages for samples with ages >1 Ga, and $^{206}Pb/^{238}U$ ages for samples with younger ages. Detrital zircon data for the Cretaceous strata in Tethyan Himalaya are from Hu *et al.* (2010) and Wang *et al.* (2011). Detrital zircons from Xigaze forearc basin are after Wu *et al.* (2010). Age data of 219 igneous rocks samples (<250 Ma) from the Lhasa terrane is given in the Table S4 (e.g. Wen *et al.*, 2008; Ji *et al.*, 2009; Zhu *et al.*, 2011a and references therein). Detrital zircons older than 250 Ma from the Lhasa terrane are after Zhu *et al.* (2011b).

The youngest zircons (52.4 ± 0.9 Ma, 53 ± 2 Ma, 54 ± 1 Ma) (Table S2) in the Enba Formation constrain the depositional age of the strata to be younger than late Ypresian, which is consistent with foraminifera data by Zhu *et al.* (2005). The youngest zircon ages in the Zhaguo Formation are 43.1 ± 0.8 Ma (one grain with two spot analyses), 49 ± 1 Ma, 52 ± 1 Ma, which suggest that the depositional age of the Zhaguo Formation is probably younger than middle Lutetian. Detrital zircon U–Pb age data further indicate that the unconformity between the Zhaguo and Enba formations may represent a hiatus of at least 7 Myr or even longer.

Detrital zircon Hf isotopes

The Lu-Hf isotope system applied to zircon is an effective provenance tool because this system is relatively stable during later tectono-thermal events and can provide additional insights into the geological history of the source rocks (e.g. Wu *et al.*, 2007). In contrast to U-Pb isotopic crystallization ages, Lu-Hf isotopes can provide crustal formation ages for the igneous source of the dated grains. Recent studies show that combined U-Pb ages and Hf isotopes of detrital zircons can effectively constrain the sources and/or origins of detrital zircon grains in sedimentary and metasedimentary rocks in the Himalayas (Wu *et al.*, 2007, 2010; Hu *et al.*, 2010; Cai *et al.*, 2011).

Nineteen of the Early Cretaceous (132–116 Ma) zircon grains dated in the GZ-H5 sample (Jidula Formation) were analysed for Hf isotope ratios (Table S3). The ε_{Hf} (t) and model ages (T^{C}_{DM}) of this detrital zircon population ranges from −7.1 to −0.2, and from 1.2 to 1.6 Ga respectively.

We found no Hf isotopic difference of detrital zircon between the Enba and Zhaguo formations and therefore consider them together. Detrital zircon (<250 Ma) Hf isotopic analysis including 41 zircon grains from the Enba Formation (sample QMB 03 and QMB08) and 71 zircon grains from the Zhaguo Formation (sample QMB16) can be separated into four populations of detrital zircon grains, based on their ε_{Hf} (t) values (see Fig. 10a; Tables 2, S2 and S3).

Group 1 zircons are dominant (80–83%) in both the Enba and Zhaguo formations, and have the youngest U–Pb ages in the Enba Formation, ranging from 53 to 121 Ma, with positive ε_{Hf} (t) of −2.6 *ca.* +16.5 and T^{C}_{DM} model ages of 0.1 *ca.* 1.3 Ga. In the Zhaguo Formation, this group of zircons have ages between 49 and 124 Ma, with positive ε_{Hf} (t) of −4.2 *ca.* +15.2 and T^{C}_{DM} model ages of 0.2–1.4 Ga. The origin of these zircons is consistent with a predominantly depleted mantle magma source as indicated by their positive ε_{Hf} (t) values.

Group 2 zircons are represented by a minor population (3–5%) in both the Enba and Zhaguo formations, and have U–Pb ages ranging from 189 to 200 Ma in the Enba Formation, with positive ε_{Hf} (t) of +10.8 to +14.8, and T^{C}_{DM} model ages of 0.6–1.5 Ga. Within this group are two zircons (181 and 182 Ma) in the Zhaguo Formation with positive ε_{Hf} (t) of +11.6 to +13.4, and T {\rm {C DM}} Z model ages of 0.4–0.5 Ga. Positive ε_{Hf} (t) values indicated that this group's origin is most likely from a predominantly depleted mantle source for the parent magma.

Group 3 zircons are a subordinate population (8–10%) in both the Enba and Zhaguo formations, with U–Pb ages ranging from 162 to 217 Ma in the Enba Formation, negative ε_{Hf} (t) of −9.2 to −2.4, and T^{C}_{DM} model ages of 1.4–1.8 Ga. In the Zhaguo Formation, zircons of this group ranges in age from 158 to 217 Ma, with negative ε_{Hf} (t) of −14.7 to −1.4, and T^{C}_{DM} model ages of 0.3–1.7 Ga. Negative ε_{Hf} (t) indicates a chemically evolved magma source, such as that produced by repeated melting of continental crust (Griffin *et al.*, 2000).

Group 4 zircons are a minor population (2%) in the Enba Formation and a subordinate population (8%) in the Zhaguo Formation. One 130 Ma zircon in the Enba Formation

Table 2. Four groups of detrital zircons distinguished by U–Pb–Hf ratios from the Enba and Zhaguo formations and their potential sources

Group		Enba Formation (QMB 03 and 08)					Zhaguo Formation (QMB16)					
		Age (Ma)	Epsilon Hf	T (DM)	Grains No.	Percent (%)	Age (Ma)	Epsilon Hf	T (DM)	Grains No.	Percent (%)	Potential source
1	Max	121	16.5	1.3	34	83	124	15.2	1.4	57	80	Southern Lhasa (Cretaceous-Paleogene)
	Min	53	−2.6	0.1			49	−4.2	0.19			
2	Max	200	14.8	1.5	2	5	182	13.4	0.49	2	3	Southern Lhasa (Late Triassic – Early Jurassic)
	Min	189	10.8	0.6			181	11.6	0.37			
3	Max	217	−2.4	1.8	4	10	217	−1.4	1.72	6	8	Central Lhasa (Triassic – Jurassic)
	Min	162	−9.2	1.4			158	−14.7	0.3			
4	Max	130	−4.7	1.5	1	2	140	−2.6	2.1	6	8	Central Lhasa or Tethyan Himalaya
	Min						115	−14.2	1.4			

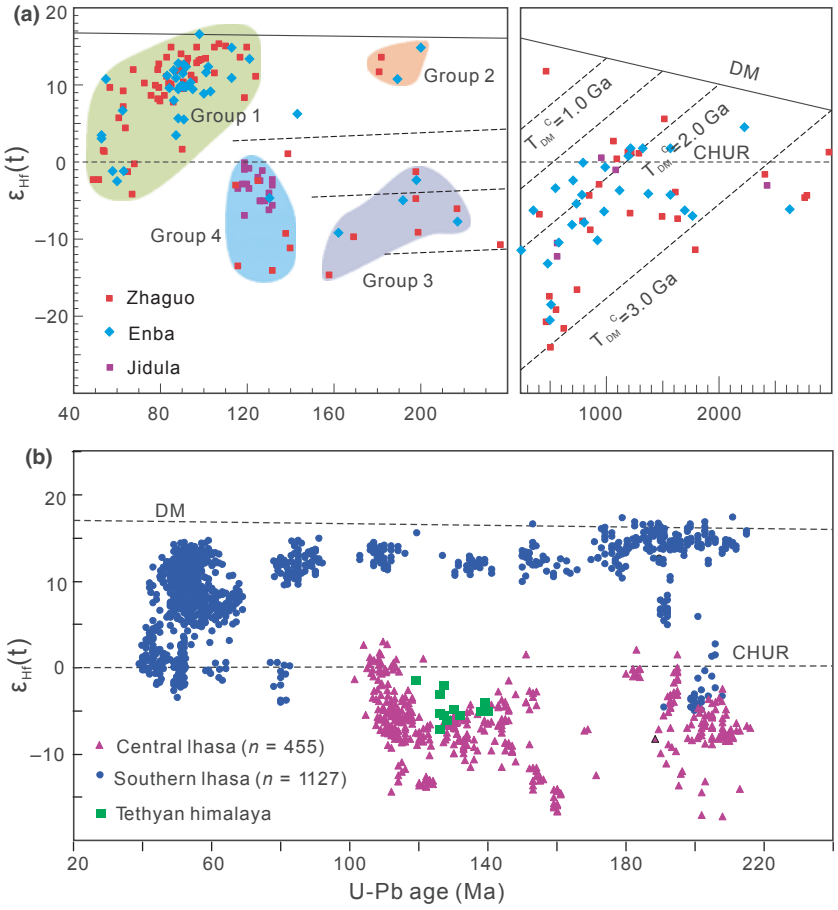

Fig. 10. Plot of $\varepsilon_{Hf}(t)$ vs. U-Pb age of analysed zircons. (a) data from the Jidula, Enba, and Zhaguo formations. Detrital zircon (<250 Ma) from the Enba and Zhaguo formations can be separated into four groups based on their $\varepsilon_{Hf}(t)$ values (see Table 2). (b) Compilation of data from the southern Lhasa (Chu *et al.*, 2006; Lee *et al.*, 2007; Zhang *et al.*, 2007a; Ji *et al.*, 2009; Zhu *et al.*, 2009b, 2011a), central Lhasa (Chu *et al.*, 2006; Zhang *et al.*, 2007b; Zhu *et al.*, 2011a), and Tethyan Himalaya (Hu *et al.*, 2010) (see Table S5).

has $\varepsilon_{Hf}(t)$ of −4.7 and T_{DM}^{C} model ages of 1.5 Ga. In the Zhaguo Formation, zircons of this group ranges in age from 115 to 140 Ma with negative $\varepsilon_{Hf}(t)$ of −14.2 to −2.6, and T_{DM}^{C} model ages of 1.4–2.1 Ga. Their $\varepsilon_{Hf}(t)$ indicate mixing of magma derived from melting a chemically evolved crust with a melt produced from melting a more chemically depleted material (Griffin *et al.*, 2000).

DISCUSSION

Sandstone provenance interpretation

Mesozoic–Cenozoic zircon isotopic properties of the Lhasa terrane and Tethyan Himalaya

Zircon crystallization ages and Hf isotopic compositions differ significantly between the Lhasa terrane and the Tethyan Himalaya (e.g. Hu *et al.*, 2010; Cai *et al.*, 2011; Zhu *et al.*, 2011b). The Lhasa terrane is composed largely of Late Triassic to Early Tertiary arc rocks, whereas the Tethyan Himalaya consists primarily of variably metamorphosed Proterozoic–Eocene strata with minor Miocene leucogranites. In this study, we concentrated on Mesozoic zircons (<250 Ma) as during Pre–Mesozoic time Lhasa and India may have had similar geological histories as they were both parts of Gondwanaland (Yin & Harrison, 2000; Zhu *et al.*, 2009b).

Recently, numerous radiometric ages have been reported (mainly zircon U–Pb ages) from intrusive and volcanic rocks in the Lhasa terrane, which allowed the establishment of a detailed geochronology database. In our database, 219 samples of intrusive and volcanic rocks have reliable SHRIMP or LA–ICPMS zircon ages from the Lhasa terrane (Wen *et al.*, 2008; Ji *et al.*, 2009; Zhu *et al.*, 2011a and references therein; see Table S4), which show that four magmatic episodes occurred from Late Triassic through Miocene: 175–216, 80–109, 41.5–69 and 21–13.5 Ma (Fig. 9). Among them, 70–41 Ma is the most widely distributed period of the magmatism, during which time the southern Gangdese batholith and Linzizong volcanic rocks were formed. The Lhasa terrane experienced two magmatic gaps at 80–69 and 41–21 Ma based on reduced zircon populations (Fig. 9); this is similar to the results of Chung *et al.* (2005), Wen *et al.* (2008) and Ji *et al.* (2009).

Detrital zircon analysed from Upper Cretaceous strata deposited in the Lhasa terrane shows similar zircon age populations to the database of granites and volcanic rocks.

392 of 547 detrital zircons from the Cretaceous Xigaze forearc basin are of Mesozoic age (*ca.* 73%) with the largest population between 77 and 140 Ma and a second population between 140 and 200 Ma (Wu *et al.*, 2010). 293 detrital zircons from Upper Cretaceous sandstones of the Takena Formation deposited in the Gangdese retro-arc basin, in the southern Gangdese sub-terrane (Leier *et al.*, 2007a) show the largest population of Early Cretaceous age, with ages generally between 105 and 140 Ma (peak at 120 Ma) (Leier *et al.*, 2007b). Early Jurassic zircons with ages between 180 and 200 Ma form a subordinate group within the Mesozoic population.

Detrital zircons from the Tethyan Himalaya have ages broadly clustered around *ca.* 500 and *ca.* 1100 Ma, with lesser peaks at *ca.* 1500–1700 and *ca.* 2500 Ma (DeCelles *et al.*, 2000, 2004; Gehrels *et al.*, 2003). A group of Early Cretaceous (*ca.* 140–*ca.* 120 Ma) detrital zircons were reported recently in the sandstones of Lower Cretaceous Wölong Volcaniclastics at Gucuo area, Tingri (Hu *et al.*, 2010; Fig. 1b), which are the only Mesozoic zircon population in the Tethyan Himalaya (Fig. 9). These Early Cretaceous detrital zircons were suggested to have come from coeval Lower Cretaceous volcanic rocks, which were situated along the northern Greater Indian margin (Garzanti, 1993, 1999; Jadoul *et al.*, 1998; Hu *et al.*, 2010). The volcanic rocks of the Sangxiu and Comei formations (*ca.* 132 Ma) in southeastern Tibet (Zhu *et al.*, 2009a) are other indicators of Early Cretaceous magmatism at the northern margin of the Greater India.

In our database, Hf values of 1127 zircons from southern Lhasa and 455 zircons from central Lhasa with ages of <250 Ma available from the intrusive and volcanic rocks (Fig. 10b; Table S5) reveal three distinct groups of zircon: (1) Late Triassic – Palaeogene age (215–39 Ma) zircons with positive $\varepsilon_{Hf}(t) > 0$ indicating mainly mantle sources; (2) Late Triassic – Early Jurassic age (216–180 Ma) with strong negative $\varepsilon_{Hf}(t)$ of −14–−2; and (3) latest Jurassic – Early Cretaceous (160–101 Ma) negative $\varepsilon_{Hf}(t)$ of −17–+3. The $\varepsilon_{Hf}(t)$ of the Early Cretaceous zircons (n = 12) from the sandstones of Wölong Volcaniclastics in Tethyan Himalaya range from −1.5 to −7.2 (Fig. 10b; Hu *et al.*, 2010).

Provenance interpretation

Detrital zircon U–Pb age and Hf isotopic ratios confirm that the provenance of the Jidula Formation is sourced from the Indian craton to the south, indicated by the similarities in U–Pb age distribution and Hf isotopic ratios with zircons from the Tethyan Himalaya, and particularly those from the Lower Cretaceous Wölong Volcaniclastics (Hu *et al.*, 2010) (Figs 9 and 10).

U–Pb ages and Hf isotopic ratios indicate that the Group 1 of the Enba and Zhaguo formations probably originated from Cretaceous and Palaeogene rocks of the southern Lhasa terrane, including the Gangdese batholith (Wen *et al.*, 2008; Ji *et al.*, 2009) and the Linzizong volcanic rocks (Lee *et al.*, 2007; Mo *et al.*, 2008). Group 2 originated from the Jurassic rocks in southern Lhasa terrane represented by the Yeba Group (Chu *et al.*, 2006; Zhu *et al.*, 2008). Group 3 may have been derived from the central Lhasa terrane, which formed when Proterozoic crust of the Lhasa terrane melted during the Early Jurassic, producing abundant igneous zircons that later were incorporated into the Cretaceous S-type plutons (Chu *et al.*, 2006; Zhu *et al.*, 2011a); Group 4 may have been derived from the central Lhasa terrane (e.g. Zhu *et al.*, 2011a) or from Lower Cretaceous magmatic rocks of the northern margin of Greater India (Hu *et al.*, 2010).

Thus, detrital zircon isotope data strongly support that the sedimentary rocks of both the Enba and Zhaguo formations have similar provenance, with the main sources being rocks of the Lhasa terrane. This confirms previous suggestions that the Enba Formation records the first appearance of detritus from the Asian margin (Wang *et al.*, 2002a; Zhu *et al.*, 2005; Najman *et al.*, 2010). We consider the source, at least of the zircons with Cretaceous–early Eocene U–Pb ages, which comprise 83% of the detrital zircon population (Table 2), to be most likely derived from the southern Lhasa terrane of Asian plate, rather than the Dazhuqu–Baingang–Zedong intraoceanic arc and ophiolites (Aitchison *et al.*, 2007), because U–Pb ages of zircons that have been dated from the intraoceanic arc indicate that it is Late Jurassic or older (McDermid *et al.*, 2002); zircons of such age in the Enba and Zhaguo formations are rare.

Evolution of an Eocene foreland basin

The provenance data from the Zhepure Mountain demonstrate that the first appearance of orogenic detritus from Asia occurred around 50.6 Ma (P8, Zhu *et al.*, 2005), when the siliciclastic rocks of upper part of the Enba Formation were deposited (Fig. 5). The subsidence curves indicate a period of relative accelerated subsidence during accumulation of the Enba Formation (Fig. 8). We suggest that the rocks of the upper part of the Enba Formation would represent a foredeep basin depositing in a storm-affected outer shelf environment connected to the deforming thrust wedge to the north (Fig. 11).

The Zhaguo Formation had been deposited in fluvial environment, which most probably represents a wedge-top basin (Fig. 11), when parts of underlying Enba Formation or its equivalent strata were accreted into the thrust wedge and erosionally reworked as a provenance source to the Zhaguo Formation. Reworking of the Enba Formation is evidenced by the microfossils described previously and by the similar U–Pb age population and Hf isotopes of detrital zircons (Figs 9 and 10).

The unconformity between the Enba and the overlying Zhaguo formations (50.6 to <43.1 Ma (youngest zircons) would correspond to the transition from the marine to nonmarine sedimentation in the foreland basin (e.g. Heller *et al.*, 1988; Sinclair, 1997b). It is proposed that the unconformity records the transition from marine foredeep, to nonmarine sedimentation in a wedge-top basin. Similar successions of deformed marine strata unconformably

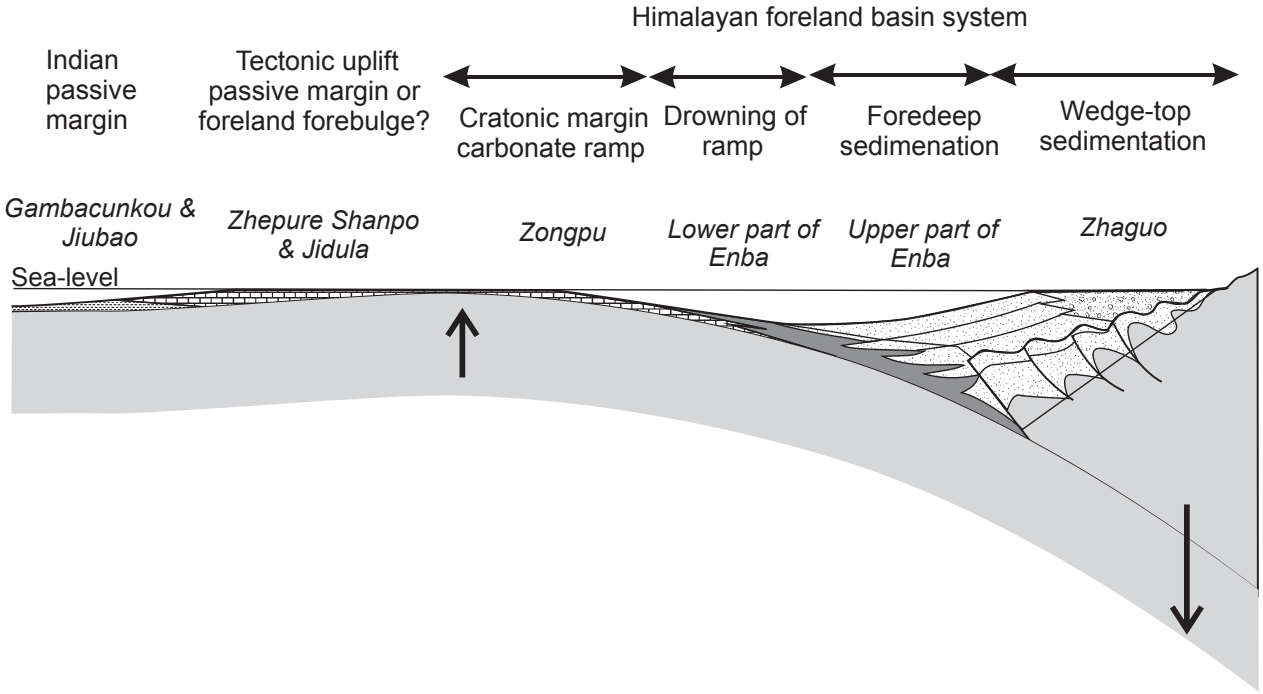

Fig. 11. Cartoon showing the interpreted evolutionary model for the tectonic and stratigraphic development of the early Himalayan foreland basin interpreted in the Zhepure Mountain area of southern Tibet.

overlain by wedge-top nonmarine sedimentary rocks are well recorded in the Palaeogene Tremp basin of the southern Pyrenees (Puigdefàbregas & Souquet, 1986; Mellere, 1993). An alternative interpretation is that this unconformity may be related to the Eocene Neo-Tethyan slab break-off, as suggested by the studies of Gangdese batholiths and Linzizong volcanic rocks (Chung *et al.*, 2005; Wen *et al.*, 2008; Ji *et al.*, 2009; Lee *et al.*, 2009). However, the clear angular discordance suggests initial structural deformation of the Enba Formation by folding and thrusting prior to deposition of the Zhaguo Formation.

Tectonic setting of the Palaeogene carbonate platform (Zongpu Fm.)

There has been debate concerning the tectonic setting on the Palaeogene carbonate platform in the Tethyan Himalaya, southern Tibet. The most accepted model is that the Indian passive margin basin continued from Palaeozoic up to the Eocene time (Searle *et al.*, 1987; Gaetani & Garzanti, 1991; Rowley, 1996, 1998), where the Zongpu Formation was taken as the latest deposits of the Indian passive margin.

Alternately, the distal margin of underfilled foreland basins is a favoured site for the accumulation of large carbonate platforms (Pigram *et al.*, 1989; Barnolas & Teixell, 1994; Dorobek, 1995; Sinclair, 1997a; Galewsky, 1998; Kirkham, 1998; Proust *et al.*, 1998; Bosence, 2005). The controls on the recurrence of platforms in this location relate to their isolation from major siliciclastic supply in an extensive area of marine shelf generated in response to flexural loading by the orogenic wedge on the proximal side of the basin. The geometry of the flexural profile creates accommodation space that encourages the development of carbonate ramps. Our data demonstrate that during late Danian–Ypresian time (Zongpu Formation), a carbonate ramp was established which recorded an overall transgressive trend from inner to middle ramp environments. The lower part of the Enba Formation records hemi-pelagic sedimentation beyond the direct effect of wave energy, and deep enough that no large benthic foraminifera are preserved. This deepening into a more distal ramp setting is consistent with the acceleration of flexurally induced subsidence having outpaced carbonate production on the ramp, but still on a northwardly dipping slope such that orogenic detritus does not yet accumulate in this part of the basin.

Discussion on latest Cretaceous-earliest Palaeogene tectonic uplift

The latest Cretaceous-earliest Palaeogene tectonic uplift in Zhepure Mountain area was represented by the shallowing stratigraphic record during the deposition of the Zhepure Shanpo and Jidula formations. The global sea level change at this time interval (Miller *et al.*, 2005; Kominz *et al.*, 2008) varies less than 70 m and so cannot explain the magnitude of signal recorded by the succession in Zhepure Mountain. Moreover, the corrected subsidence curve (Fig. 8) suggests that the Indian passive margin experienced absolute uplift for about 10 Myr in a submarine setting during accumulation of the Zhepure Shanpo and Jidula formations. We provide two possible explanations for the probable signal of tectonic uplift of the northern Indian passive margin basin prior to the accelerated basin subsidence: (1) tectonic uplift repre-

sented by mantle-plume upwelling; (2) flexure forebulge related either to oceanic subduction, continental collision, or ophiolite obduction.

Model 1: tectonic uplift generated by mantle-plume upwelling

A prediction of mantle-plume theory is the upward displacement of the Earth's surface in response to heating approximately 10–20 Myr before flood volcanism, when the top of the plume head is still well below the lithosphere (e.g. Rainbird & Ernst, 2001; Campbell, 2005; Cande & Stegman, 2011). Up to now, there was no evidence of a Late Cretaceous hotspot near Tingri in the Tethyan Himalaya. However, the Réunion hotspot in India (*ca.* 1300 km away from the Tingri area) is an archetypal deep mantle plume with a plume head that arrived firstly at the Earth's surface around 67–68 Myr ago, erupting the flood basalts around the Cretaceous-Tertiary boundary that formed the Deccan traps (see Chenet *et al.*, 2007 and references therein). Is it possible that Tingri was located above the Réunion hotspot during latest Cretaceous time when the tectonic uplift is recorded? Plate reconstructions based on palaeomagnetic data suggest that the Indian plate attained a very high speed (18–20 cm yr^{-1}) during the Late Cretaceous epoch) (e.g. Klootwijk *et al.*, 1992; Copley *et al.*, 2010; van Hinsbergen *et al.*, 2011), which implies that the India plate would have drifted northward over 1800–2000 km within 10 Ma before the Deccan flood volcanism erupted, assuming that the Réunion hotspot was stable. If we take the 600 km as the shortening distance between Tingri and the Himalayan frontal trust (DeCelles *et al.*, 2002), the original distance from Tingri to Deccan traps would be approximately 1900 km. Therefore, it is feasible that the uplift found in the Tingri area was driven by the Réunion hotspot; this should be viewed as a speculative hypothesis at this stage.

Model 2: tectonic uplift generated by plate flexure related to oceanic subduction, continental collision or ophiolite obduction

Flexure of the distal Indian margin may have occurred when the flexural profile of the subducted oceanic lithosphere was translated onto the margins of the Indian continental plate; in this scenario, the initial flexure of the outer Indian plate would record uplift in a forebulge region of the profile. Flexure of the Indian margin may also produce a history of elevation change related either to early plate collision and initiation of a foreland basin or to ophiolite obduction. A prediction from the foreland basin model is that prior to the first accumulation of sediment derived from a northerly, Asian source (i.e. the Enba Formation), we may expect evidence of flexural responses to loading in the region of the passive margin (DeCelles & Giles, 1996; Sinclair, 1997a). In this model, the transition from hemipelagic marls and limestones of the Gambacunkou and Jiubao formations into the shallowing trend of the Zhepure Shanpo and Jidula formations culminating in a near coastal setting would be interpreted as a record of a passive margin setting being uplifted by a rising forebulge during the onset of lithospheric flexure. Depending on the inherited depth of the passive margin, the height of the forebulge may not be sufficient for it to emerge above sea level and thus no subaerial erosion may occur (Crampton & Allen, 1995). The disconformity from the pelagic, outer shelf environment of Jiubao Formation to the turbiditic slope environment of Zhepure Shanpo Formation may thus indicate the initial upward flexure and instability of the Indian plate.

Similarly, flexural induced uplift followed by accelerated subsidence may have occurred when ophiolites obducted over the Indian passive margin acting as a tectonic load (Searle *et al.*, 1997). In the western Himalaya, it has been proposed that ophiolitic rocks were obducted onto the northwestern margin of India during latest Cretaceous–earliest Tertiary time (Searle *et al.*, 1987, 1997; Beck *et al.*, 1996), although this model was debated and challenged for over the past decades (see Kelemen *et al.*, 1988; Guillot *et al.*, 2003; Garzanti *et al.*, 2005). However, there is no solid evidence to support ophiolite obduction in southern Tibet during this time interval, although Ding *et al.* (2005) dated hornblende from mafic schists in the Yarlung Zangbo mantle thrust at *ca.* 63 Ma and suggested that it may be linked to ophiolite obduction.

Considering that the Indian plate drifted at 18–20 cm yr^{-1} during the Late Cretaceous epoch (Klootwijk *et al.*, 1992; Copley *et al.*, 2010; van Hinsbergen *et al.*, 2011), the duration of tectonic uplift represented by a forebulge which resulted from either oceanic subduction, continental collision or from ophiolite obduction would depend on its width, and hence the flexural rigidity. In the simplest flexural case of a sinusoidal continuous plate model, the forebulge would be twice the width of the downward flexure of the basin, and greater for a broken plate (Turcotte and Schubert, 1982). At the above rates, and a duration of 10 Myr, the region of uplift would need to be approximately 1800 km wide. Therefore, we view the uplift and subsidence history of the Tingri sections as either being a record of early collisional processes, or linked to thermal anomalies in the mantle.

Discussion on the timing of India-Asia initial collision

In Tingri, the youngest marine facies and the Asian detritus occurred in the Enba Formation which was dated about 50 Ma (Wang *et al.*, 2002a; Zhu *et al.*, 2005; Najman *et al.*, 2010; this study). The cessation of marine facies deposition represents the starting of land-to-land (hard) collision time and provides a minimum age for initial collision. Several studies on collisional orogens indicated that marine sedimentation may continue for several to tens of millions of years after the subducting continental margin was initially overthrust at its distal margin (e.g. Miall, 1995; Sinclair, 1997a; Allen & Allen, 2005). Therefore, the stratigraphic signal for India-Asia

initial collision would be expected to be preserved in the strata which underlie the Enba Formation.

In this context, the Zongpu Formation would be interpreted as a carbonate ramp which occupied the submarine forebulge position in the distal foreland basin system. If this interpretation is correct (see more discussion in the Appendix S1), the India–Asia initial collision should have occurred before the deposition of the Zongpu carbonate ramp, which is dated by foraminifera as late Danian (*ca.* 62 Ma) (Wan *et al.*, 2002). This conclusion is supported by new palaeomagnetic data in central Himalaya suggesting that the initial contact between the Tethyan Himalaya and Lhasa terrane was established before 60 Ma while the Zongpu Formation would be a part of post-collisional deposits (Tong *et al.*, 2008; YI *et al.*, 2011). This age of *ca.* 62 Ma for initial collision was coeval with the age of India–Asia faunal exchange (Wan *et al.*, 2002) and possible initiation of deformation of the Indian margin (Searle *et al.*, 1987; Ratschbacher *et al.*, 1994; Beck *et al.*, 1996; Ding *et al.*, 2005), and formation and exhumation of eclogites related to continental subduction (e.g. Leech *et al.*, 2005).

Palaeogene continental deformation in the Lhasa terrane and the Xigaze forearc basin may be used to constrain the India–Asia collision (Appendix S1). In the Xigaze forearc basin, a basin-wide, angular unconformity occurred between the overlying Palaeogene Cuojiangding Group and the underlying folded Upper Cretaceous Qubeiya Formation and Xigaze Group (Einsele *et al.*, 1994; Wang *et al.*, 1999; Ding *et al.*, 2005). Similarly, in the Linzhou basin near Lhasa, a widespread (over 1100 km along strike) angular unconformity occurred between the Takena Formation and the Tertiary Linzizong volcanic succession (e.g. Pan *et al.*, 2006; Mo *et al.*, 2007). Moreover, Palaeogene intracontinental shorting has been recorded along the Gangdese retroarc thrust belt (Kapp *et al.*, 2007) and the northern Lhasa terrane thrust belt (Kapp *et al.*, 2003, 2005; Volkmer *et al.*, 2007), as well as further to the north of Lhasa terrane, such as in the Nangquan-Yushu area (e.g. Horton *et al.*, 2002; Spurlin *et al.*, 2005), in the Hoh Xil area (e.g. Liu *et al.*, 2001; Wang *et al.*, 2002b), in the Qaidam and West Qinlin areas (Yin *et al.*, 2008; Clark *et al.*, 2010) and in the Dangchang-Xining- Minghe area in northeast Tibet (e.g. Horton *et al.*, 2004).

CONCLUSIONS

(1) The sedimentology of the Upper Cretaceous and Palaeogene succession of the Zhepure Mountains, southern Tibet records an initial shallowing (Zhepure Shanpo and Jidula formations) with the establishment of a carbonate ramp (Zongpu Formation), which then records deepening into a hemipelagic setting (lower part of the Enba Formation). The upper part of the Enba Formation records deposition of a storm-influenced outer shelf. An abrupt upward transition from outer shelf of the Enba Formation into nonmarine fluvial strata of the Zhaguo Formation completes the succession in this region.

(2) Detrital zircon and U–Th–Hf isotope data from sandstones in the succession indicate that the Jidula Formation was sourced from the Indian margin, whereas the upper part of the Enba Formation was sourced from the Asian margin at approximately 50 Ma. The Zhaguo Formation indicates a high degree of recycling from the underlying Enba Formation, which is supported by microfossil analysis.

(3) Backstripped subsidence analysis indicates that the shallowing during latest Cretaceous-earliest Palaeocene time (Zhepure Shanpo and Jidula formations) was driven by relative uplift of basement, followed by stability (Zongpu Formation) until early Eocene time when accelerated subsidence occurred (Enba Formation).

(4) The stratigraphic, sedimentological, provenance and subsidence data suggest that the Enba and Zhaguo formations were parts of the early Himalayan foreland basin. The Enba Formation was deposited in a foredeep basin while the youngest nonmarine Zhaguo Formation was deposited in a wedge-top basin. Palaeoenvironmental analysis indicates that the Zongpu Formation was a deepening-upward carbonate ramp, which occupied a submarine forebulge region in a distal foreland basin. If this interpretation is correct, the India–Asia initial collision must have happened before the late Danian (*ca.* 62 Ma) when the Zongpu Formation deposited.

(5) The corrected subsidence curve suggests clearly that tectonic uplift of basement rocks (the Indian passive margin) during accumulation of the Zhepure Shanpo and Jidula formations occurred for about 10 Myr in a submarine setting. This uplift would be either be represented by mantle-plume upwelling or the passage of a flexural forebulge related to oceanic subduction, continental collision or ophiolite obduction.

ACKNOWLEDGEMENTS

This work benefited through the years from numerous fruitful discussions with Chengshan Wang, Xiaoqiao Wan, Xuanxue Mo, Dicheng Zhu, Guobiao Li, Xianghui Li, Lihui Chen, Jingen Dai, Zhicheng Huang, Luba Jansa, Helmut Willems, Yani Najman, Amy Weislogel. We thank Jinhai Yu, Lijuan Wang, and Bin Wu for their assistance in the lab, and Cong Wu, Wei An, Gaoyuan Sun for their help in the field. The first author (X. Hu) acknowledges affective collaboration at the University of Edinburgh as visiting scholar during the years of 2010–2011. Reviewers E. Garzanti, A. Carter, an anonymous reviewer, and associate editor B. Horton are gratefully acknowledged for their stimulating and constructively reviews and helpful comments. This study was financially

supported by the MOST 973 Project (2011CB822001), the NSFC Project (41172092, 40772070), and Grant from the State Key Laboratory for Mineral Deposits Research, Nanjing University.

APPENDIX S1

IMPLICATION OF PALEOGENE HIMALAYAN FORELAND BASIN

Based on our stratigraphic, sedimentological, provenance and subsidence data, we proposed that at least the Palaeogene strata (the Zongpu, Enba and Zhaguo formations) were syncollisional and were part of an early stage of the Himalayan foreland basin. However, this interpretation meets several challenges. The first challenge is the requirement of a topographic load to drive plate flexure. In the proposed model, a zone of latest Cretaceous – Palaeogene shortening and crustal thickening should be recorded in southern Tibet. In fact, continental deformation does occur during latest Cretaceous time in the Lhasa terrane and the Xigaze forearc basin. In the Xigaze forearc basin, this deformation is represented by the basin-wide, angular unconformity between the overlying Tertiary Cuojiangding Group and the underlying folded Upper Cretaceous Qubeiya Formation and Xigaze Group (Einsele *et al.*, 1994; Wang *et al.*, 1999; Ding *et al.*, 2005). Similarly, in the Linzhou basin near Lhasa, the latest Cretaceous deformation is expressed in the folding of the Upper Cretaceous Takena Formation and the widespread (over 1100 km along strike) angular unconformity between the Takena Formation and the Tertiary Linzizong volcanic succession (e.g. Pan *et al.*, 2006; Mo *et al.*, 2007). Moreover, the Palaeogene magmatism such as the Linzizong volcanic succession and Gangdese batholiths was suggested to make an important role in Cenozoic crust thickening of the Lhasa block (Mo *et al.*, 2007). Those authors further suggested that the mantle material input through magmatism contributed about 30% of the total thickness of the present-day Tibetan crust. This significant thickness of the Lhasa lithosphere will contribute to the topographic load required by the foreland flexure.

The second challenge for this interpretation of the India–Asia initial collision is the amount of subsequent intracontinental shortening required. Early India–Asia collision at *ca.* 62 Ma predicts at least 1200 km of convergence and significant intercontinental shortening between 62 and 50 Ma based on the relative convergence rate between India and Asia (e.g. Guillot *et al.*, 2003; Copley *et al.*, 2010). The apparent absence of Palaeocene shortening in southern Tibet (Burg *et al.*, 1983; England & Searle, 1986) challenges this interpretation. However, a few facts should be considered before ruling out this possibility: (1) As stated above, there was deformation and the formation of regional unconformities during latest Cretaceous time both in the Xigaze forearc area and southern Lhasa (Einsele *et al.*, 1994; Wang *et al.*, 1999; Ding *et al.*, 2005; Mo *et al.*, 2007). (2) Palaeogene intracontinental shorting has been recorded along the Gangdese retroarc thrust belt (Kapp *et al.*, 2007) and the northern Lhasa terrane thrust belt (Kapp *et al.*, 2003, 2005; Volkmer *et al.*, 2007), as well as further to the north of Lhasa terrane, such as in the Nangquan–Yushu area (e.g. Horton *et al.*, 2002; Spurlin *et al.*, 2005), the Hoh Xil area (e.g. Liu *et al.*, 2001; Wang *et al.*, 2002b), the Qaidam and West Qinlin areas (Yin *et al.*, 2008; Clark *et al.*, 2010) and Dangchang–Xining–Minghe area in northeast Tibet (e.g. Horton *et al.*, 2004). For example, detailed cross-section restorations indicated a minimum of *ca.* 43% shortening in the Yushu–Nangqian thrust belt during the Palaeogene (Spurlin *et al.*, 2005); Similarly shortening rate of *ca.* 45% was given in the Tanggula thrust belts near the Hoh Xil basin (Wang *et al.*, 2002b). (3) The early record of crustal shortening of the Indian margin could have been either subducted beneath the Lhasa block along the Indus–Yarlung suture zone or within the Greater India as suggested by van Hinsbergen *et al.* (2011) or eroded away during later orogenic evolution, or simply not recorded by any studies to date.

SUPPORTING INFORMATION

Additional Supporting Information may be found in the online version of this article:

Fig. S1. Characteristic microfacies from the Qumiba B section, Zhepure Mountain, south Tibet. (a) MF-Q1, Floatstone with nummulitids mainly represented by *Miscellanea* and *Ranikothalia*. Sample 09QMB3-3. (b) MF-Q2, Floatstone with alveolinids and small benthic foraminifera (mainly rotaliids and miliolids). Sample 09QMB3-5. (c) MF-Q3 Floatstone with *Alveolina* and *Nummulites.* Sample 09QMB50-8. (d) MF-Q4 Floatstone with *Nummulites* and *Alveolina*. Sample 09QMB5-12; MF-Q5 Floatstone (e, sample 09QMB5-14) or rudstone (f, sample 09QMB6-4) with *Assilina* and *Discocyclina* and minor *Nummulites.* (g) Oolitic limestones, sample 06QMB04. (h) shell-rich bioclastic limestones, sample 06QMB05 in the middle of the Enba Formation. Both ooids and mixed bioclastic debris are reworked with terrigenous materials. Abbreviation: Alveo. – *Alveolina;* Assi. – *Assilina*; Disco. – *Discocyclina;* Num. – *Nummulites*; mil. – miliolids; Rani. – *Ranikothalia*; orbi. – *Orbitolites.*

Fig. S2. Concordia diagrams for detrital zircon U-Pb ages used in spectra plots.

Fig. S3. Planktonic foraminifera distribution from the Gelamu section, Zhepure Mountain (from Wu *et al.*, 2011).

Table S1. Microfacies of the Zongpu Formation in the Zhepure Mountain, southern Tibet

Table S2. Analysed detrital zircon U-Pb age data from the Zhepure Mountain, southern Tibet

Table S3. Analysed detrital zircon Hf isotope data from the Zhepure Mountain, southern Tibet

Table S4. Published U-Pb age data of intrusive and volcanic rocks in the Lhasa terrane

Table S5. Published Hf isotopic data from dated zircons in the southern Lhasa terrane, central Lhasa terrane and Tethyan Himalaya terrane

Please note: Wiley-Blackwell are not responsible for the content or functionality of any supporting materials supplied by the authors. Any queries (other than missing material) should be directed to the corresponding author for the article.

REFERENCES

Achache, J., Courtillot, V. & Zhou, Y.X. (1984) Paleogeographic and tectonic evolution of southern Tibet since middle cretaceous time – new paleomagnetic data and synthesis. *J. Geophys. Res.*, **89**, 311–339.

Aitchison, J.C., Davis, A.M., Badengzhu, B. & Luo, H. (2002) New constraints on the India-Asia collision: the Lower Miocene Gangrinboche conglomerates, Yarlung Tsangpo suture zone, Se Tibet. *J. Asian Earth Sci.*, **21**, 251–263.

Aitchison, J.C., McDermid, I.R.C., Ali, J.R., Davis, A.M. & Zyabrev, S.V. (2007) Shoshonites in southern Tibet record Late Jurassic rifting of a Tethyan Intraoceanic island arc. *J. Geol.*, **115**, 197–213.

Ali, J.R. & Aitchison, J.C. (2008) Gondwana to Asia: plate tectonics, paleogeography and the biological connectivity of the Indian sub-continent from the Middle Jurassic through latest Eocene (166-35 Ma). *Earth-Sci. Rev.*, **88**, 145–166.

Allen, P.A. & Allen, J.R. (2005) *Basin Analysis: Principles and Applications*. Wiley-Blackwell, Oxford, UK.

Barnolas, A. & Teixell, A. (1994) Platform sedimentation and collapse in a carbonate-dominated margin of a foreland basin (Jaca basin, Eocene, southern Pyrenees). *Geology*, **22**, 1107–1110.

Beck, R.A., Burbank, D.W., Sercombe, W.J., Khan, A.M. & Lawrence, R.D. (1996) Late Cretaceous ophiolite obduction and Paleocene India-Asia collision in the western-most Himalaya. *Geodin. Acta*, **9**, 114–144.

Bosence, D. (2005) A genetic classification of carbonate platforms based on their basinal and tectonic settings in the Cenozoic. *Sed. Geol.*, **175**, 49–72.

Burg, J.P., Proust, F., Tapponnier, P. & Chen, G.M. (1983) Deformation phases and tectonic evolution of the Lhasa block (southern Tibet, China)= Déformation Des Phases Et Évolution Tectonique Du Bloc Lhasa, Tibet Sud, Chine. *Eclogae Geol. Helv.*, **76**, 643–665.

Cai, F.L., Ding, L. & Yue, Y.H. (2011) Provenance analysis of upper Cretaceous strata in the Tethys Himalaya, southern Tibet: implications for timing of India-Asia collision. *Earth Planet. Sci. Lett.*, **305**, 195–206.

Campbell, I.H. (2005) Large igneous provinces and the mantle plume hypothesis. *Elements*, **1**, 265–269.

Cande, S.C. & Stegman, D.R. (2011) Indian and African plate motions driven by the push force of the reunion plume head. *Nature*, **475**, 47–52.

Cawood, P.A., Johnson, M.R.W. & Nemchin, A.A. (2007) Early Palaeozoic orogenesis along the Indian margin of Gondwana: tectonic response to Gondwana assembly. *Earth Planet. Sci. Lett.*, **255**, 70–84.

Chen, J.S., Huang, B.C. & Sun, L.S. (2010) New constraints to the onset of the India-Asia collision: paleomagnetic reconnaissance on the Linzizong Group in the Lhasa Block, China. *Tectonophysics*, **489**, 189–209.

Chenet, A.L., Quidelleur, X., Fluteau, F., Courtillot, V. & Bajpai, S. (2007) 40 K-40 Ar dating of the Main Deccan large igneous province: further evidence of Ktb age and short duration. *Earth Planet. Sci. Lett.*, **263**, 1–15.

Chu, M.F., Chung, S.L., Song, B.A., Liu, D.Y., O'Reilly, S. Y., Pearson, N.J., Ji, J.Q. & Wen, D.J. (2006) Zircon U-Pb and Hf isotope constraints on the Mesozoic tectonics and crustal evolution of southern Tibet. *Geology*, **34**, 745–748.

Chung, S.L., Chu, M.F., Zhang, Y.Q., Xie, Y.W., Lo, C.H., Lee, T.Y., Lan, C.Y., Li, X.H., Zhang, Q. & Wang, Y.Z. (2005) Tibetan tectonic evolution inferred from spatial and temporal variations in post-collisional magmatism. *Earth-Sci. Rev.*, **68**, 173–196.

Clark, M.K., Farley, K.A., Zheng, D.W., Wang, Z.C. & Duvall, A.R. (2010) Early Cenozoic faulting of the northern Tibetan plateau margin from apatite (U-Th)/He ages. *Earth Planet. Sci. Lett.*, **296**, 78–88.

Copley, A., Avouac, J.P. & Royer, J.Y. (2010) India-Asia collision and the Cenozoic slowdown of the Indian plate: implications for the forces driving plate motions. *J. Geophys. Res. Solid Earth*, **115**, B03410, doi:10.1029/2009JB006634.

Crampton, S.L. & Allen, P.A. (1995) Recognition of forebulge unconformities associated with early stage foreland basin development; example from the North Alpine Foreland Basin. *AAPG Bulletin.*, **79**, 1495–1514.

Critelli, S. & Ingersoll, R.V. (1994) Sandstone petrology and provenance of the Siwalik Group (northwestern Pakistan and western-southeastern Nepal). *J. Sed. Res.*, **64**, 815–823.

DeCelles, P.G. & Giles, K.A. (1996) Foreland basin systems. *Basin Res.*, **8**, 105–123.

DeCelles, P.G., Gehrels, G.E., Quade, J. & Ojha, T.P. (1998a) Eocene early Miocene foreland basin development and the history of Himalayan thrusting, western and central Nepal. *Tectonics*, **17**, 741–765.

DeCelles, P.G., Gehrels, G.E., Quade, J., Ojha, T.P., Kapp, P.A. & Upreti, B.N. (1998b) Neogene foreland basin deposits, erosional unroofing, and the kinematic history of the Himalayan fold-thrust belt, western Nepal. *Geol. Soc. Am. Bull.*, **110**, 2–21.

DeCelles, P.G., Gehrels, G.E., Quade, J., LaReau, B. & Spurlin, M. (2000) Tectonic implications of U-Pl Zircon ages of the Himalayan orogenic belt in Nepal. *Science*, **288**, 497–499.

DeCelles, P.G., Robinson, D.M. & Zandt, G. (2002) Implications of shortening in the Himalayan fold-thrust belt for uplift of the Tibetan Plateau. *Tectonics*, **21**, 1062. doi:10.1029/2001TC001322.

DeCelles, P.G., Gehrels, G.E., Najman, Y., Martin, A.J., Carter, A. & Garzanti, E. (2004) Detrital geochronology and geochemistry of Cretaceous-Early Miocene strata of Nepal: implications for timing and diachroneity of initial Himalayan orogenesis. *Earth Planet. Sci. Lett.*, **227**, 313–330.

DeCelles, P.G., Kapp, P., Quade, J. & Gehrels, G.E. (2011) Oligocene-Miocene Kailas basin, southwestern Tibet: record of postcollisional upper-plate extension in the Indus-Yarlung suture zone. *Geol. Soc. Am. Bull.*, **123**, 1337–1362.

Ding, L., Kapp, P. & Wan, X.Q. (2005) Paleocene-Eocene record of ophiolite obduction and initial India-Asia collision, South central Tibet. *Tectonics*, **24**. doi:10.1029/2004TC001729.

Dorobek, S.L. (1995) Synorogenic carbonate platforms and reefs in foreland basins: controls on stratigraphic evolution and platform/reef morphology. In: *Stratigraphic Evolution of Foreland Basins* (Ed. by S.L. Dorobek & G.M. Ross) *SEPM Spec. Publ.*, **52**, 127–148.

Dubois-Cote, V., Hebert, R., Dupuis, C., Wang, C.S., Li, Y. L. & Dostal, J. (2005) Petrological and geochemical evidence for the origin of the Yarlung Zangbo ophiolites, southern Tibet. *Chem. Geol.*, **214**, 265–286.

Dupont-Nivet, G., Lippert, P.C., van Hinsbergen, D.J.J., Meijers, M.J.M. & Kapp, P. (2010) Palaeolatitude and age of the Indo-Asia collision: palaeomagnetic constraints. *Geophys. J. Int.*, **182**, 1189–1198.

Dürr, S.B. (1996) Provenance of Xigaze fore-arc basin clastic rocks (Cretaceous, South Tibet). *Geol. Soc. Am. Bull.*, **108**, 669–684.

Einsele, G., Liu, B., Dürr, S., Frisch, W., Liu, G., Luterbacher, H.P., Ratschbacher, L., Ricken, W., Wendt, J., Wetzel, A., Yu, G. & Zheng, H. (1994) The Xigaze forearc basin: evolution and facies architecture (Cretaceous, Tibet). *Sed. Geol.*, **90**, 1–32.

England, P. & Searle, M. (1986) The Cretaceous-Tertiary deformation of the Lhasa block and its implications for crustal thickening in Tibet. *Tectonics*, **5**, 1–14.

Gaetani, M. & Garzanti, E. (1991) Multicyclic history of the northern India continental margin (northwestern Himalaya). *AAPG Bulletin.*, **75**, 1427–1446.

Galewsky, J. (1998) The dynamics of foreland basin carbonate platforms: tectonic and eustatic controls. *Basin Res.*, **10**, 409–416.

Gansser, A. (1964) *Geology of the Himalayas*. Interscience Publishers, London, UK.

Garzanti, E. (1993) Sedimentary evolution and drowning of a passive margin shelf (Giumal Group; Zanskar Tethys Himalaya, India); palaeoenvironmental changes during final breakup of Gondwanaland. *Geol. Soc. Spec. Publ.*, **74**, 277–298.

Garzanti, E. (1999) Stratigraphy and sedimentary history of the Nepal Tethys Himalaya passive margin. *J. Asian Earth Sci.*, **17**, 805–827.

Garzanti, E. (2008) Comment On "When and where did India and Asia collide?" by Jonathan C. Aitchison, Jason R. Ali, and Aileen M. Davis. *J. Geophys. Res. Solid Earth*, **113**. doi:10.1029/2007JB005276, 002008.

Garzanti, E., Baud, A. & Mascle, G. (1987) Sedimentary record of the northward flight of India and its collision with Eurasia (Ladakh Himalaya, India). *Geodin. Acta*, **1**, 297–312.

Garzanti, E., Sciunnach, D., Gaetani, M., Corfield, R.I., Watts, A.B. & Searle, M.P. (2005) Discussion on subsidence history of the North Indian continental margin, Zanskar-Ladakh Himalaya, NW India. *J. Geol. Soc.*, **162**, 889–892.

Gehrels, G.E., DeCelles, P.G., Martin, A., Ojha, T.P., Pinhassi, G. & Upreti, B.N. (2003) Initiation of the Himalayan orogen as an early Paleozoic thin-skinned thrust belt. *GSA Today*, **13**, 4–9.

Gradstein, F.M., Ogg, J.G., Smith, A.G., Agterberg, F.P., Bleeker, W., Cooper, R.A., Davydov, V., Gibbard, P., Hinnov, L.A., House, M.R., Lourens, L., Luterbacher, H. P., Mcarthur, J., Melchin, M.J., Robb, L.J., Shergold, J., Villeneuve, M., Wardlaw, B.R., ALI, J., Brinkhuis, H., Hilgen, F.J., Hooker, J., Howarth, R.J., Knoll, A.H., Laskar, J., Monechi, S., Powell, J., Plumb, K.A., Raffi, I ., Röhl, U., Sanfilippo, A., Schmitz, B., Shackleton, N.J., Shields, G.A., Strauss, H., Van dam, J., Veizer, J., Van Kolfschoten, T. & Wilson, D. (2004) *A Geologic Time Scale 2004*. Cambridge University Press, Cambridge, UK.

Griffin, W.L., Pearson, N.J., Belousova, E., Jackson, S.E., van Achterbergh, E., O'Reilly, S.Y. & Shee, S.R. (2000) The Hf isotope composition of cratonic mantle: Lam-Mc-Icpms analysis of zircon megacrysts in kimberlites. *Geochim. Cosmochim. Acta*, **64**, 133–147.

Guillot, S., Garzanti, E., Baratoux, D., Marquer, D., Maheo, G. & de Sigoyer, J. (2003) Reconstructing the total shortening history of the NW Himalaya. *Geochem. Geophy. Geosy.*, **4**, 1064, doi:10.1029/2002GC000484.

Hao, Y. & Wan, X. (1985) The marine Cretaceous and Tertiary strata of Tingri, Xizang (Tibet). *Contrib. Geol. Qinghai-Xizang (Tibet)*, **17**, 227–332.

Heller, P.L., Angevine, C.L., Winslow, N.S. & Paola, C. (1988) Two-phase stratigraphic model of foreland-basin sequences. *Geology*, **16**, 501–504.

Heron, A.M. (1922) Geological results of the Mount Everest reconnaissance expedition. *Reccord Geol. Surv. India*, **54**, 215–234.

van Hinsbergen, D.J.J., Steinberger, B., Doubrovine, P.V. & Gassmoller, R. (2011) Acceleration and deceleration of India-Asia convergence since the cretaceous: roles of mantle plumes and continental collision. *J. Geophys. Res. Solid Earth*, **116**, B06101, doi: 10.1029/2010JB008051.

Hodges, K.V. (2000) Tectonics of the Himalaya and southern Tibet from two perspectives. *Geol. Soc. Am. Bull.*, **112**, 324–350.

Horton, B.K., Yin, A., Spurlin, M.S., Zhou, J.Y. & Wang, J. H. (2002) Paleocene-Eocene syncontractional sedimentation in narrow, lacustrine-dominated basins of east-central Tibet. *Geol. Soc. Am. Bull.*, **114**, 771–786.

Horton, B.K., Dupont-Nivet, G., Zhou, J., Waanders, G.L., Butler, R.F. & Wang, J. (2004) Mesozoic-Cenozoic evolution of the Xining-Minhe and Dangchang basins, northeastern Tibetan Plateau: magnetostratigraphic and biostratigraphic results. *J. Geophys. Res.*, **109**, 1–15.

Hu, X., Jansa, L. & Wang, C. (2008) Upper Jurassic-Lower Cretaceous stratigraphy in south-eastern Tibet: a comparison with the western Himalayas. *Cretaceous Res.*, **29**, 301–315.

Hu, X., Jansa, L., Chen, L., Griffin, W.L., O'Reilly, S.Y. & Wang, J. (2010) Provenance of lower cretaceous W Long volcaniclastics in the Tibetan Tethyan Himalaya: implications for the final breakup of eastern Gondwana. *Sed. Geol.*, **223**, 193–205.

Huang, B.C., Chen, J.S. & Yi, Z.Y. (2010) Paleomagnetic discussion of when and where India and Asia initially collided. *Chin. J. Geophy. Chin. Ed.*, **53**, 2045–2058.

Jackson, S.E., Pearson, N.J., Griffin, W.L. & Belousova, E. A. (2004) The application of laser ablation-inductively coupled plasma-mass spectrometry to *in situ* U/Pb zircon geochronology. *Chem. Geol.*, **211**, 47–69.

Jadoul, F., Berra, F. & Garzanti, E. (1998) The Tethys Himalayan passive margin from Late Triassic to Early Cretaceous (South Tibet). *J. Asian Earth Sci.*, **16**, 173–194.

Ji, W.Q., Wu, F.Y., Chung, S.L., Li, J.X. & Liu, C.Z. (2009) Zircon U-Pb geochronology and Hf isotopic constraints on

petrogenesis of the Gangdese batholith, southern Tibet. *Chem. Geol.*, **262**, 229–245.

Kapp, P., Murphy, M.A., Yin, A., Harrison, T.M., Ding, L. & Guo, J.H. (2003) Mesozoic and Cenozoic tectonic evolution of the Shiquanhe area of western Tibet. *Tectonics*, **22**, 1029, doi:10.1029/2001TC001332.

Kapp, P., Yin, A., Harrison, T.M. & Ding, L. (2005) Cretaceous-Tertiary shortening, basin development, and volcanism in central Tibet. *Geol. Soc. Am. Bull.*, **117**, 865–878.

Kapp, P., DeCelles, P., Leier, A., Fabijanic, J., He, S., Pullen, A., Gehrels, G. & Ding, L. (2007) The Gangdese retroarc thrust belt revealed. *GSA Today*, **17**, 4–9, doi: 10.1130/GSAT01707A.01701.

Kelemen, P.B., Reuber, I. & Fuchs, G. (1988) Structural evolution and sequence of thrusting in the High Himalayan, Tibetan-Tethys and Indus suture zones of Zanskar and Ladakh, western Himalaya – discussion. *J. Struct. Geol.*, **10**, 129–130.

Kirkham, A. (1998) A Quaternary proximal foreland ramp and its continental fringe, Arabian Gulf, UAE. *Geol. Soc. London Spec. Publ.*, **149**, 15–41.

Klootwijk, C.T., Gee, J.S., Peirce, J.W., Smith, G.M. & McFadden, P.L. (1992) An early India-Asia contact; paleomagnetic constraints from Ninetyeast Ridge, Odp Leg 121; with Suppl. Data 92-15. *Geology*, **20**, 395–398.

Kominz, M.A., Browning, J.V., Miller, K.G., Sugarman, P. J., Mizintseva, S. & Scotese, C.R. (2008) Late Cretaceous to Miocene sea-level estimates from the New Jersey and Delaware coastal plain coreholes: an error analysis. *Basin Res.*, **20**, 211–226.

Le Fort, P. (1989) The Himalayan orogenic segment. In: *Tectonic Evolution of the Tethyan Region*, Vol. **259** (Ed. by A.M. C. Sengör), pp. 289–386. Kluwer Academic Publishers, Norwell, Massachusetts.

Lee, H.Y., Chung, S.L., Wang, Y.B., Zhu, D.C., Yang, J.H., Song, B., Liu, D. & Wu, F.Y. (2007) Age, petrogenesis and geological significance of the Linzizong volcanic successions in the Linzhou basin, southern Tibet: evidence from Zircon U–Pb Dates and Hf isotopes. *Acta Petrologica Sinica*, **23**, 493–500.

Lee, H.Y., Chung, S.L., Lo, C.H., Ji, J.Q., Lee, T.Y., Qian, Q. & Zhang, Q. (2009) Eocene Neotethyan slab breakoff in southern Tibet inferred from the Linzizong volcanic record. *Tectonophysics*, **477**, 20–35.

Leech, M.L., Singh, S., Jain, A.K., Klemperer, S.L. & Manickavasagam, R.M. (2005) The onset of India-Asia continental collision: early, steep subduction required by the timing of UHP metamorphism in the western Himalaya. *Earth Planet. Sci. Lett.*, **234**, 83–97.

Leier, A.L., DeCelles, P.G., Kapp, P. & Ding, L. (2007a) The Takena Formation of the Lhasa terrane, southern Tibet: the record of a Late Cretaceous retroarc foreland basin. *Geol. Soc. Am. Bull.*, **119**, 31–48.

Leier, A.L., Kapp, P., Gehrels, G.E. & DeCelles, P.G. (2007b) Detrital zircon geochronology of Carboniferous–Cretaceous strata in the Lhasa terrane, Southern Tibet. *Basin Res.*, **19**, 361–378.

Li, X., Jenkyns, H.C., Wang, C., Hu, X., Chen, X., Wei, Y., Huang, Y. & Cui, J. (2006) Upper Cretaceous carbon- and oxygen-isotope stratigraphy of hemipelagic carbonate facies from southern Tibet, China. *J. Geol. Soc. London*, **163**, 375–382.

Liebke, U., Appel, E., Ding, L., Neumann, U., Antolin, B. & Xu, Q.A. (2010) Position of the Lhasa terrane prior to India-Asia collision derived from palaeomagnetic inclinations of 53 Ma old dykes of the Linzhou basin: constraints on the age of collision and post-collisional shortening within the Tibetan plateau. *Geophys. J. Int.*, **182**, 1199–1215.

Lippert, P.C., Zhao, X.X., Coe, R.S. & Lo, C.H. (2011) Palaeomagnetism and Ar-40/Ar-39 geochronology of upper palaeogene volcanic rocks from central Tibet: implications for the central Asia inclination anomaly, the palaeolatitude of Tibet and Post-50 Ma shortening within Asia. *Geophys. J. Int.*, **184**, 131–161.

Liu, J.B. & Aitchison, J.C. (2002) Upper Paleocene radiolarians from the Yamdrok melange, South Xizang (Tibet), China. *Micropaleontology*, **48**, 145–154.

Liu, G. & Einsele, G. (1994) Sedimentary history of the Tethyan basin in the Tibetan Himalayas. *Geol. Rundsch.*, **83**, 32–61.

Liu, G. & Einsele, G. (1996) Various types of olistostromes in a closing ocean basin, Tethyan Himalaya (Cretaceous, Tibet). *Sed. Geol.*, **104**, 203–226.

Liu, Z.F., Wang, C.S. & Yi, H.S. (2001) Evolution and mass accumulation of the Cenozoic Hoh Xil basin, northern Tibet. *J. Sed. Res.*, **71**, 971–984.

McDermid, I.R.C., Aitchison, J.C., Davis, A.M., Harrison, T.M. & Grove, M. (2002) The Zedong terrane: a Late Jurassic intra-oceanic magmatic arc within the Yarlung-Tsangpo Suture zone, southeastern Tibet. *Chem. Geol.*, **187**, 267–277.

Mellere, D. (1993) Thrust-generated, back-fill stacking of alluvial fan sequences, South-Central Pyrenees, Spain (La Pobla De Segur Conglomerates). In: *Tectonic Controls and Signatures in Sedimentary Successions* (Ed. by L.E. Frostick & R.J. Steel) *Spec. publ. Int. Assoc. Sedimentol.*, **20**, 259–276.

Miall, A.D. (1995) Collision-related foreland basins. In: *Tectonics of Sedimentary Basins* (Ed. by C.J. Busby & R.V. Ingersoll), pp. 393–424. Blackwell Science, Oxford, UK.

Miller, K.G., Kominz, M.A., Browning, J.V., Wright, J.D., Mountain, G.S., Katz, M.E., Sugarman, P.J., Cramer, B. S., Christie-Blick, N. & Pekar, S.F. (2005) The Phanerozoic record of global sea-level change. *Science*, **310**, 1293–1298.

Mo, X., Hou, Z., Niu, Y., Dong, G., Qu, X., Zhao, Z. & Yang, Z. (2007) Mantle contributions to crustal thickening during continental collision: evidence from Cenozoic igneous rocks in southern Tibet. *Lithos*, **96**, 225–242.

Mo, X., Niu, Y., Dong, G., Zhao, Z., Hou, Z., Zhou, S. & Ke, S. (2008) Contribution of syncollisional felsic magmatism to continental crust growth: a case study of the Paleogene Linzizong volcanic succession in southern Tibet. *Chem. Geol.*, **250**, 49–67.

Mu, A., Wen, S., Wang, Y. & Chang, P. (1973) Stratigraphy of the Mount Jolmo Lungma region in southern Tibet, China. *Sci. Sinica*, **16**, 96–111.

Najman, Y., Carter, A., Oliver, G. & Garzanti, E. (2005) Provenance of Eocene foreland basin sediments, Nepal: constraints to the timing and diachroneity of early himalayan orogenesis. *Geology*, **33**, 309–312.

Najman, Y., Appel, E., Boudagher-Fadel, M., Bown, P., Carter, A., Garzanti, E., Godin, L., Han, J., Liebke, U., Oliver, G., Parrish, R. & Vezzoli, G. (2010) Timing of India-Asia collision: geological, biostratigraphic, and palaeomagnet-

ic constraints. *J. Geophys. Res.*, **115**, B12416. doi:10.1029/2010JB007673.

Pan, G.T., Mo, X.X., Hou, Z.Q., Zhu, D.C., Wang, L.Q., Li, G.M., Zhao, Z.D., Geng, Q.R. & Liao, Z.L. (2006) Spatial-temporal framework of the Gangdese Orogenic Belt and its evolution. *Acta Petrologica Sinica*, **22**, 521–533.

Patzelt, A., Li, H., Junda, W. & E., A. (1996) Palaeomagnetism of Cretaceous to Tertiary sediments from southern Tibet: evidence for the extent of the northern margin of India prior to the collision with Eurasia. *Tectonophysics*, **259**, 259–284.

Pigram, C.J., Davies, P.J., Feary, D.A. & Symonds, P.A. (1989) Tectonic controls on carbonate platform evolution in southern Papua New Guinea: passive margin to foreland basin. *Geology*, **17**, 199–202.

Proust, J.N., Chuvashov, B.I., Vennin, E. & Boisseau, T. (1998) Carbonate platform drowning in a foreland setting; the Mid-Carboniferous platform in western Urals (Russia). *J. Sed. Res.*, **68**, 1175–1188.

Puigdefàbregas, C. & Souquet, P. (1986) Tecto-sedimentary cycles and depositional sequences of the Mesozoic and Tertiary from the Pyrenees. *Tectonophysics*, **129**, 173–203.

Rainbird, R.H. & Ernst, R.E. (2001) The sedimentary record of mantle-plume uplift. In: Mantle Plumes: Their Identification through Time (Ed. by R.E. Ernst & K.L. Buchan), Vol. **352**, pp. 227–246. Geological Society of America Speical Paper, Boulder, Colorado.

Ratschbacher, L., Frisch, W., Liu, G. & Chen, C. (1994) Distributed deformation in southern and western Tibet during and after the India-Asia collision. *J. Geophys. Res.*, **99**, 19917–19945.

Rowley, D.B. (1996) Age of initiation of collision between India and Asia: a review of stratigraphic data. *Earth Planet. Sci. Lett.*, **145**, 1–13.

Rowley, D.B. (1998) Minimum age of initiation of collision between India and Asia North of Everest based on the subsidence history of the Zhepure Mountain section. *J. Geol.*, **106**, 229–235.

Searle, M.P., Windley, B.F., Coward, M.P., Cooper, D.J.W., Rex, A.J., Rex, D., Tingdong, L., Xuchang, X., Jan, M.Q. & Thakur, V.C. (1987) The closing of Tethys and the tectonics of the Himalaya. *Geol. Soc. Am. Bull.*, **98**, 678–701.

Searle, M., Corfield, R.I., Stephenson, B. & McCarron, J. (1997) Structure of the North Indian continental margin in the Ladakh-Zanskar Himalayas: implications for the timing of obduction of the Spontang ophiolite, India-Asia collision and deformation events in the Himalaya. *Geol. Mag.*, **134**, 297–316.

Sinclair, H.D. (1997a) Tectonostratigraphic model for Underfilled peripheral foreland basins: an Alpine perspective. *Geol. Soc. Am. Bull.*, **109**, 324–346.

Sinclair, H.D. (1997b) Flysch to molasse transition in peripheral foreland basins: the role of the passive margin versus slab breakoff. *Geology*, **25**, 1123–1126.

Soederlund, U., Patchett, P.J., Vervoort, J.D. & Isachsen, C.E. (2004) The ¹⁷⁶ Lu decay constant determined by Lu-Hf and U-Pb isotope systematics of Precambrian mafic intrusions. *Earth Planet. Sci. Lett.*, **219**, 311–324.

Spurlin, M.S., Yin, A., Horton, B.K., Zhou, J. & Wang, J. (2005) Structural evolution of the Yushu-Nangqian region and its relationship to syncollisional igneous activity east-central Tibet. *Geol. Soc. Am. Bull.*, **117**, 1293–1317.

Sun, Z.M., Jiang, W., Li, H.B., Pei, J.L. & Zhu, Z.M. (2010) New paleomagnetic results of Paleocene volcanic rocks from the Lhasa block: tectonic implications for the collision of India and Asia. *Tectonophysics*, **490**, 257–266.

Tong, Y., Zheng, L., Yang, T., Shi, L. & Sun, Z. (2008) Early Paleocene paleomagnetic results from southern Tibet, and tectonic implications. *Int. Geol. Rev.*, **50**, 546–562.

Turcotte, D., Schubert, G. (1982) *Geodynamics: Applications of Continuum Mechanics to Geological Problens*. John Wiley, New York.

Volkmer, J.E., Kapp, P., Guynn, J.H. & Lai, Q.Z. (2007) Cretaceous–Tertiary structural evolution of the North central Lhasa Terrane, Tibet. *Tectonics*, **26**, TC6007, doi:10.1029/2005TC001832.

Wan, X.Q., Jansa, L.F. & Sarti, M. (2002) Cretaceous and Paleogene boundary strata in southern Tibet and their implication for the India-Eurasia collision. *Lethaia*, **35**, 131–146.

Wang, C., Liu, Z., Li, X. & Wan, X. (1999) *Xigaze Forearc Basin and Yarlung-Zangbo Suture Zone, Tibet*. Geological Publishing House, Beijing.

Wang, C.S., Li, X.H., Hu, X.M. & Jansa, L.F. (2002a) Latest marine horizon North of Qomolangma (Mt Everest): implications for closure of Tethys seaway and collision tectonics. *Terra Nova*, **14**, 114–120.

Wang, C.S., Liu, Z.F., Yi, H.S., Liu, S. & Zhao, X.X. (2002b) Tertiary crustal shortenings and peneplanation in the Hoh Xil region: implications for the tectonic history of the northern Tibetan Plateau. *J. Asian Earth Sci.*, **20**, 211–223.

Wang, J., Hu, X., Jansa, L. & Huang, Z. (2011) Provenance of the Upper Cretaceous-Eocene deep-water sandstones in Sangdanlin, southern Tibet: constraints on the timing of initial India-Asia Collision. *J. Geol.*, **119**, 293–309.

Wen, D.-R., Liu, D., Chung, S.-L., Chu, M.-F., Ji, J., Zhang, Q., Song, B., Lee, T.-Y., Yeh, M.-W. & Lo, C.-H. (2008) Zircon Shrimp U-Pb ages of the Gangdese Batholith and implications for Neotethyan subduction in southern Tibet. *Chem. Geol.*, **252**, 191–201.

Wendler, I., Wendler, J., Gr fe, K.U., Lehmann, J. & Willems, H. (2009) Turonian to Santonian carbon isotope data from the Tethys Himalaya, southern Tibet. *Cretaceous Res.*, **30**, 961–979.

Willems, H. (1993) Sedimentary history of the Tethys Himalaya continental margin in the South Tibet (Gamba, Tingri) during upper Cretaceous and Paleogene (Xizang Autonomous Region, Pr China). In: *Geoscietific Investigations in the Tethyan Himalayas*(Ed. by H. Willems) *Berichte aus dem Fachbereich Geowissenschaften, der Universit t Bremen*, **38**, 49–181.

Willems, H. & Zhang, B. (1993) Cretaceous and lower Tertiary Sediments of the Tibetan Tethys Himalaya in the area of Tingri (South Tibet, Pr China). In: *Geoscientific Investigations in the Tethyan Himalayas*(Ed. by H. Willems), *Ber. Fachbereich Geowiss. Univ. Bremen*, **38**, 29–47.

Willems, H., Zhou, Z., Zhang, B. & Grafe, K.U. (1996) Stratigraphy of the Upper Cretaceous and lower Tertiary Strata in the Tethyan Himalayas of Tibet (Tingri Area, China). *Geol. Rundsch.*, **85**, 723–754.

Wu, F.Y., Clift, P.D. & Yang, J.H. (2007) Zircon Hf isotopic constraints on the sources of the Indus Molasse, Ladakh Himalaya, India. *Tectonics*, **26**, TC2014, doi: 10.1029/2006TC002051.

Wu, F.Y., Ji, W.Q., Liu, C.Z. & Chung, S.L. (2010) Detrital Zircon U-Pb and Hf isotopic data from the Xigaze fore-arc

basin: constraints on Transhimalayan magmatic evolution in southern Tibet. *Chem. Geol.*, **271**, 13–25.

Wu, C., Shi, Y.K. & Hu, X. (2011) The disconformity in the Late Cretaceous Strata at Tingri (Southern Tibet) and its age constrained constrained by planktonic foraminifera. *Acta Micropalaeontologica Sinica*, **28**, 381–401.

Yi, Z.Y., Huang, B.C., Chen, J.C., Chen, L.W. & Wang, H.L. (2011) Paleomagnetism of early Paleogene marine sediments in southern Tibet, China: Implications to onset of the India–Asia collision and size of Greater India. *Earth Planet. Sci. Lett.*, **309**, 153–165.

Yin, A. & Harrison, T.M. (2000) Geologic evolution of the Himalayan-Tibetan orogen. *Annu. Rev. Earth Planet Sci.*, **28**, 211–280.

Yin, A., Dang, Y.Q., Wang, L.C., Jiang, W.M., Zhou, S.P., Chen, X.H., Gehrels, G.E. & McRivette, M.W. (2008) Cenozoic tectonic evolution of Qaidam basin and its surrounding regions (Part 1): the southern Qilian Shan-Nan Shan thrust belt and northern Qaidam basin. *Geol. Soc. Am. Bull.*, **120**, 813–846.

Zhang, H.F., Xu, W.C., Guo, J.Q., Zong, K.Q., Cai, H. M. & Yuan, H.L. (2007a) Zircon U–Pb and Hf isotopic composition of deformed granite in the southern margin of the Gangdese belt, Tibet: evidence for early Jurassic subduction of Neo-Tethyan oceanic slab. *Acta Petrol. Acta*, **23**, 1347–1353.

Zhang, H.F., Xu, W.C., Guo, J.Q., Zong, K.Q., Cai, H.M. & Yuan, H.L. (2007b) Indosinian orogenesis of the Gangdese terrane: evidences from zircon U–Pb dating and petrogenesis of granitoids. *Earth Sciences – J. China Univ. Geosci.*, **32**, 155–166.

Zhu, T., Zou, G. & Zhou, M. (2002) *1:250,000 Geological Map of the Nyalam Area, Tibet*. Tibet Chengdu Institute of Geology and Mineral Resources, Chengdu.

Zhu, B., Kidd, W.S.F., Rowley, D.B., Currie, B.S. & Shafique, N. (2005) Age of initiation of the India-Asia collision in the east-central Himalaya. *J. Geol.*, **113**, 265–285.

Zhu, D.C., Pan, G.T., Chung, S.L., Liao, Z.L., Wang, L.Q. & Li, G.M. (2008) Shrimp zircon age and geochemical constraints on the origin of Lower Jurassic volcanic rocks from the Yeba Formation, southern Gangdese, South Tibet. *Int. Geol. Rev.*, **50**, 442–471.

Zhu, D.C., Chung, S.L., Mo, X.X., Zhao, Z.D., Niu, Y., Song, B. & Yang, Y.H. (2009a) The 132 Ma Comei-Bunbury large igneous province: remnants identified in present-day southeastern Tibet and southwestern Australia. *Geology*, **37**, 583–586.

Zhu, D.C., Mo, X.X., Niu, Y., Zhao, Z.D., Wang, L.Q., Liu, Y. S. & Wu, F.Y. (2009b) Geochemical investigation of early cretaceous igneous rocks along an east-west traverse throughout the central Lhasa Terrane, Tibet. *Chem. Geol.*, **268**, 298–312.

Zhu, D.C., Zhao, Z.D., Niu, Y., Mo, X.X., Chung, S.L., Hou, Z.Q., Wang, L.Q. & Wu, F.Y. (2011a) The Lhasa Terrane: record of a microcontinent and its histories of drift and growth. *Earth Planet. Sci. Lett.*, **301**, 241–255.

Zhu, D.-C., Zhao, Z.-D., Niu, Y., Dilek, Y. & Mo, X.-X. (2011b) Lhasa terrane in southern Tibet came from Australia. *Geology*, **39**, 727–730.

Manuscript received 13 February 2011; In revised form 05 December 2011; Manuscript accepted 06 January 2012.

